



### **Science Arts & Métiers (SAM)**

is an open access repository that collects the work of Arts et Métiers Institute of Technology researchers and makes it freely available over the web where possible.

This is an author-deposited version published in: <https://sam.ensam.eu>  
Handle ID: <http://hdl.handle.net/10985/20655>

#### **To cite this version :**

Haitao TIAN, Michel POTIER-FERRY, Farid ABED-MERAÏM - Buckling and wrinkling of thin membranes by using a numerical solver based on multivariate Taylor series - International Journal of Solids and Structures - Vol. 230-231, p.111165 - 2021

Any correspondence concerning this service should be sent to the repository

Administrator : [scienceouverte@ensam.eu](mailto:scienceouverte@ensam.eu)



# Buckling and wrinkling of thin membranes by using a numerical solver based on multivariate Taylor series

H. Tian<sup>a,b</sup>, M. Potier-Ferry<sup>a,1,\*</sup>, F. Abed-Meraim<sup>a</sup>

<sup>a</sup>*Université de Lorraine, CNRS, Arts et Métiers ParisTech, LEM3, F-57000 Metz, France*

<sup>b</sup>*Guangdong Technion-Israel Institute of Technology, 241 Daxue Road, Shantou, Guangdong, 515063 China*

---

## Abstract

Buckling and wrinkling of thin structures often lead to very complex response curves that are hard to follow by standard path-following techniques, especially for very thin membranes in a slack or nearly slack state. Many recent papers mention numerical difficulties encountered in the treatment of wrinkling problems, especially with path-following procedures and often these authors switch to pseudo-dynamic algorithms. Moreover, the numerical modeling of many wrinkles leads to very large size problems. In this paper, a new numerical procedure based on a double Taylor series is presented, that combines path-following techniques and discretization by a Trefftz method: Taylor series with respect to a load parameter (Asymptotic Numerical Method) and with respect to space variables (Taylor Meshless Method). The procedure is assessed on buckling benchmarks and on the difficult problem of a sheared rectangular membrane.

---

\*michel.potier-ferry@univ-lorraine.fr

*Keywords:*

wrinkling, buckling, Trefftz method, asymptotic numerical method, Taylor meshless method

---

## 1. Introduction

There was recently a very strong interest within the scientific community in thin membrane structures and their instabilities. The numerical simulation of such elastic sheets is not an easy task when they are very thin. Generally, path-following algorithms are appropriate tools to solve the associated nonlinear boundary value problems, especially with an arc-length control [1] [2][3], which is often referred to Riks method. If these procedures are very efficient for standard buckling problems (e.g.[4]), they may fail in cases of very thin structures, say when the aspect ratio is larger than 1000, which is mainly due to a vanishing bending stiffness and to the coexistence of too many equilibrium solutions. Moreover the size of the numerical model may be very large if one simulates many wrinkles with a shell finite element code, for instance to capture the appearance of complex patterns as those obtained experimentally for film-substrate systems [5].

There are alternative procedures to circumvent the lack of reliability of path-following techniques and the excessive size of the numerical models, which extends the arsenal of available numerical techniques, but each one has generally a few shortcomings. One of the earliest is the tension-field theory [6][7][8] that allows distinguishing three coexisting states of a membrane

(slack, wrinkled, taut), but disregards the features of the wrinkles. On the contrary, with the Fourier Fast Transform [9][10], many wrinkles can be described in details but only with periodicity conditions and this does not allow accounting for any wrinkling appearing near the boundary. A quite different Fourier-related approach [11] is able to solve various boundary problems with a low computational cost, but there are few restrictive assumptions, the main one being a prescribed and uniform wavevector. Thus it remains important to improve the numerical techniques for solving accurately nonlinear boundary value problems discretized by generic techniques like the finite element method. In this respect, there exist well established procedures to detect bifurcation points, for instance by solving the extended system characterizing these bifurcations [12], or by computing a bifurcation indicator [13][14] or by post-processing a Taylor series [15][16], but such bifurcation analyses have to come after and before a standard path-following technique. Dynamic relaxation [7][17][18][19][20] is one of the most reliable procedures to provide a solution for these difficult nonlinear static systems: one has to define an artificial dynamical system whose large time response provides the searched equilibria. Here, the drawback is the difficulty to characterize the numerous hysteresis loops that may give an overview of the whole set of equilibrium solutions.

The recent literature reports several typical benchmarks illustrating the numerical difficulties encountered in the treatment of these intricate boundary value problems. A very representative case is the problem of a rectangular

thin sheet under shear loading that was discussed by Wong and Pellegrino, experimentally [21], theoretically [22] and numerically [23]. Roughly, a path-following technique would generally permit to compute the wrinkled states that are characterized by a tensile stress much larger than the compressive one, but these two principal stresses are nearly identical in the case of the sheared membrane: so it is difficult to capture these patterns corresponding to nearly slack states. Initially, this problem was considered too difficult to be solved by a path following method and the dynamic relaxation was applied to solve a modified version that was stabilized by a rather large transverse tension [23]. In another paper [7], very large shears were applied, which is an alternative manner to stabilize the membrane. More recently, other authors [24][25][26] were able to solve this shear problem with commercial computer codes by using classical Newton-like procedures, but always with the help of large transverse tension. In the present paper, this iconic benchmark is revisited with the help of an efficient path-following algorithm and by trying to disregard the additional tensile load. Another benchmark was recently revisited: a spherical film-substrate system that was studied both by dynamic relaxation and Riks method [27]. In this reference [27], the pseudo-dynamic technique proves to be robust, while the Riks method generally diverges during the post-bifurcation regime. Note that there are other interesting results about this wrinkling problem of spherical system in [28][29], with assessment concerning shell finite element, reduced modeling and comparison between path-following and dynamic procedures. Despite of these failures, one may

wonder if continuation techniques are necessarily unable to solve nearly slack membrane problems.

The purpose of this paper is to establish a numerical method based on a path-following technique and able, first to solve the difficult problems posed by the wrinkling of very thin membranes, second to reduce significantly the number of degrees of freedom with respect to classical discretization techniques, as finite element or finite difference methods. The nonlinear solver will be the Asymptotic Numerical Method (ANM). ANM relies on Taylor series with respect to a path parameter [30] [31] [32][33], each step-length is related to the radius of convergence of the series and therefore it can be defined after the computation of the series, which leads to naturally adaptive step-lengths and makes easier the control of strongly nonlinear solution curves. It has been applied to a lot of models, including non-smooth mechanics [34] and large scale problems [35] [16]. Thus ANM seems well adapted to membrane wrinkling analyses because of this step length adaptivity, ensuring the reliability of continuation of calculations.

ANM has to be associated with a classical discretization technique that was most often the finite element method, but also sometimes meshless methods, such as Moving Least-Squares [36], Method of Fundamental Solution [37] or spectral method [38]. In order to reduce the size of the discrete model, the Taylor Meshless Method (TMM) has been chosen, the reduction of the number of degrees of freedom (DOFs) being obtained by analytical solving of the Partial Differential Equations (PDEs) in the form of Taylor series. In

this respect, TMM belongs to the family of Trefftz methods [39][40] that are characterized by the use of exact or quasi-exact solutions of the PDEs. So, there are many variants of Trefftz methods that are mainly distinguished by the chosen shape functions: harmonic polynomials [41][42], wave-based functions [43], fundamental solutions [44][45] and many others [46], several papers being devoted to plate bending [41][47]. TMM was introduced in [48] and various techniques for boundary and transmission conditions are available with a Taylor series per subdomain [49][50][40]. The computation of Taylor series to solve quasi-exactly the PDEs is the heart of these Taylor-based methods. This relies on well-established differentiation techniques [51][52] that permit to carry out the computation of the series for almost all systems of equations [53][54]. Moreover, the procedure involves only boundary variables, which is much more difficult to be obtained with other variants of Trefftz methods. Note that it was tacitly admitted that Trefftz methods were not able to solve large scale problems because of matrix ill-conditioning [55], but carefully chosen splittings in subdomains have permitted to efficiently solve numerical problems requiring several millions of DOFs in an equivalent finite element model, at least in the cases of wave-based functions [43] and of Taylor series [56][54].

In this paper, one applies both Asymptotic Numerical Method, because of a very robust path-following technique, and Taylor Meshless Method, because of strong reductions of the number of DOFs. The considered model was the well-known Föppl-von Karman plate equation. It is limited to small

membrane strains and this is not too restrictive in cases of very thin membranes. Thus, multivariate Taylor expansions were used: a power series with respect to a scalar parameter representing the load (ANM) and another power series with respect to the space variables in each subdomain (TMM). It is worth noting that a preliminary report of this research was published in a short paper [57]. The in-plane displacement was disregarded in that previous paper, what limited its possible applications. Moreover, the study of the buckling problem in section 3.2 and the wrinkling problem in section 4 are new.

The paper is organized as follows. All the numerical procedures are presented in section 2. Next, two basic plate buckling problems will be discussed in order to assess the numerical method, especially in the neighborhood of bifurcation points (section 3). Last, in section 4, one rediscusses the wrinkling of a very thin rectangular plate submitted to shear loading that is a typical example of the difficulties encountered in solving thin membrane problems by a path-following algorithm. Moreover, one tries to carry out this computation without the regularization effect of a transverse tension.

## 2. A numerical method based on double Taylor series

The aim is to solve the Föppl-von Karman (FvK) plate equations [58][59] that are here expressed in terms of the deflection  $w(x, y)$  and of the stress function  $f(x, y)$ , the latter being related to the membrane forces (or stress resultants) by  $N_{xx} = \frac{\partial^2 f}{\partial y^2}$ ,  $N_{yy} = \frac{\partial^2 f}{\partial x^2}$ ,  $N_{xy} = -\frac{\partial^2 f}{\partial x \partial y}$ . The applied loads are only



transversal and written as  $\lambda p(x, y)$ , where the function  $p(x, y)$  is given and the scalar  $\lambda$  is the load parameter. The load parameter  $\lambda$  can also be defined from the boundary conditions. When expressed in terms of stress function, FvK equations can be written in a simple form involving two bilaplacian operators:

$$\begin{cases} D\Delta^2 w - [w, f] = \lambda p \\ \frac{1}{Eh}\Delta^2 f + \frac{1}{2}[w, w] = 0, \end{cases} \quad (1)$$

where the bracket operator involves the second derivatives of its arguments:

$$[A, B] = \frac{\partial^2 A}{\partial x^2} \frac{\partial^2 B}{\partial y^2} + \frac{\partial^2 A}{\partial y^2} \frac{\partial^2 B}{\partial x^2} - 2 \frac{\partial^2 A}{\partial x \partial y} \frac{\partial^2 B}{\partial x \partial y}. \quad (2)$$

The material and geometrical data are Young's modulus  $E$ , Poisson's ratio  $\nu$ , plate thickness  $h$  and flexural rigidity  $D = Eh^3/12(1 - \nu^2)$ . If the FvK equations (1) are beautiful, they are not convenient to apply various boundary conditions and it is interesting to re-introduce the in-plane components of the displacement  $u$  and  $v$ , which can be done via the following relations:

$$\begin{cases} \gamma_{xx} = \frac{\partial u}{\partial x} + \frac{1}{2} \left( \frac{\partial w}{\partial x} \right)^2 = \frac{1}{Eh} \left( \frac{\partial^2 f}{\partial y^2} - \nu \frac{\partial^2 f}{\partial x^2} \right) \\ \gamma_{yy} = \frac{\partial v}{\partial y} + \frac{1}{2} \left( \frac{\partial w}{\partial y} \right)^2 = \frac{1}{Eh} \left( \frac{\partial^2 f}{\partial x^2} - \nu \frac{\partial^2 f}{\partial y^2} \right) \\ 2\gamma_{xy} = \frac{\partial u}{\partial y} + \frac{\partial v}{\partial x} + \frac{\partial w}{\partial x} \frac{\partial w}{\partial y} = -\frac{1}{Gh} \frac{\partial^2 f}{\partial x \partial y}, \end{cases} \quad (3)$$

the latter equations (3) representing, first the displacement-strain relation

within FvK approximation, second the linear isotropic constitutive law. The shear modulus is classically given by  $G = E/2(1+\nu)$ . It will be interesting to use notations of Voigt type by representing the linearized strain by a column vector  $\{\epsilon(\mathbf{u})\}$  where  $\mathbf{u}$  stands for  $(u, v)$ , the plane compliance tensor by a matrix  $[M]$ , the gradient of the deflection  $w$  by a vector  ${}^t\{g\} = \left\{ \frac{\partial w}{\partial x}, \frac{\partial w}{\partial y} \right\}$ , the tensorial product  $\nabla w \otimes \nabla w$  by a product matrix $\times$ vector  $[A(\mathbf{g})]\{g\}$  and the tensor of the second derivatives by a vector  $\{D^2 f\}$ :

$$\{\epsilon\} = \begin{Bmatrix} \epsilon_{xx} \\ \epsilon_{yy} \\ 2\epsilon_{xy} \end{Bmatrix}, \quad [M] = \begin{bmatrix} -\frac{\nu}{Eh} & \frac{1}{Eh} & 0 \\ \frac{1}{Eh} & -\frac{\nu}{Eh} & 0 \\ 0 & 0 & -\frac{1}{Gh} \end{bmatrix} \quad (4)$$

$$[A(\mathbf{g})] = \begin{bmatrix} g_x & 0 \\ 0 & g_y \\ g_y & g_x \end{bmatrix}, \quad \{D^2 f\} = \begin{Bmatrix} \frac{\partial^2 f}{\partial x^2} \\ \frac{\partial^2 f}{\partial y^2} \\ \frac{\partial^2 f}{\partial x \partial y} \end{Bmatrix}. \quad (5)$$

With the latter notations, the membrane constitutive law (3) can be written in a vectorial form with  $\mathbf{g} = \nabla w$ :

$$\{\epsilon(\mathbf{u})\} + \frac{1}{2} [A(\mathbf{g})] \{g\} = [M] \{D^2 f\} \quad (6)$$

It will be convenient to re-write also the bracket operator in a vectorial

form:

$$[A, B] = {}^t \{D^2 A\} \begin{bmatrix} 0 & 1 & 0 \\ 1 & 0 & 0 \\ 0 & 0 & -2 \end{bmatrix} \{D^2 B\} \quad (7)$$

The FvK model is based on restrictive assumptions: linearity of the stress-strain law, linearity of the bending term  $D\Delta^2 w$  and linearization of the membrane strain (3) with respect to the in-plane displacement, the only remaining nonlinearity coming from the geometric effect due to transverse displacement  $w(x, y)$ . Thus, it is unable to account for the evolution of wrinkles for strains beyond 5 – 10% as, for instance, in the tensile rectangular plate problem discussed in [60]. Nevertheless, it remains relevant to describe losses of flatness occurring for plates undergoing rather small strains.

### 2.1. Taylor series with respect to the load (ANM)

The Asymptotic Numerical Method (ANM) computes solution branches of PDEs in the form of Taylor series with respect to a real number “ $a$ ” called path parameter. The most popular path parameter is a sort of linearized arc-length, for instance as:

$$a = \langle w - w_0, w_1 \rangle + \langle f - f_0, f_1 \rangle + (\lambda - \lambda_0)\lambda_1. \quad (8)$$

This parameter is quite similar to the one of the Riks method, it is not necessarily the optimal choice and other possibilities are discussed in [61], but it is quite secure and permits, for instance, to bypass easily limit points.

The effectiveness of the method does not seem sensitive to the choice of the bilinear form  $\langle ., . \rangle$  that is defined here as a  $L^2$ -product based on the set of collocation points introduced in section 2.3.

ANM seeks a family of solutions depending on the scalar parameter “ $a$ ”. The parameter  $\lambda$  is also expressed as a function of “ $a$ ”. First, the variables  $w(x, y)$ ,  $f(x, y)$ ,  $u(x, y)$ ,  $v(x, y)$  and the load parameter  $\lambda$  are expanded in the form of truncated power series with respect to the parameter “ $a$ ” from a known starting solution denoted as  $w_0(x, y)$ ,  $f_0(x, y)$ ,  $u_0(x, y)$ ,  $v_0(x, y)$ ,  $\lambda_0$ :

$$\begin{Bmatrix} w(x, y, a) \\ f(x, y, a) \\ u(x, y, a) \\ v(x, y, a) \\ \lambda(a) \end{Bmatrix} - \begin{Bmatrix} w_0(x, y) \\ f_0(x, y) \\ u_0(x, y) \\ v_0(x, y) \\ \lambda_0 \end{Bmatrix} = \sum_{K=1}^{N_A} a^K \begin{Bmatrix} w_K(x, y) \\ f_K(x, y) \\ u_K(x, y) \\ v_K(x, y) \\ \lambda_K \end{Bmatrix}. \quad (9)$$

Next, one substitutes the series (9) into the FvK system (1) and the definition of the path parameter (8). So, each equation appears as a power series and vanishing this power series is equivalent to vanishing the coefficients of  $a^K$ ,  $1 \leq K \leq N_A$ . This leads to a family of equations satisfied by the new unknowns that are the coefficients  $(w_K(x, y), f_K(x, y), \lambda_K)$  of the power series. Let us begin by the first term ( $K = 1$ ), which leads to a linearized system satisfied by the first term of the series :

$$\begin{cases} D\Delta^2 w_1 - [w_0, f_1] - [w_1, f_0] = \lambda_1 p \\ \frac{1}{Eh}\Delta^2 f_1 + [w_0, w_1] = 0 \\ 1 = \langle w_1, w_1 \rangle + \langle f_1, f_1 \rangle + \lambda_1^2. \end{cases} \quad (10)$$

The two first equations in (10) correspond exactly to the tangent system used in classical iterative algorithms. The third equation is scalar and it will be discussed later. At order two, the coefficients of  $a^2$  lead to:

$$\begin{cases} D\Delta^2 w_2 - [w_0, f_2] - [w_2, f_0] = \lambda_2 p + [w_1, f_1] \\ \frac{1}{Eh}\Delta^2 f_2 + [w_0, w_2] = -\frac{1}{2}[w_1, w_1] \\ 0 = \langle w_2, w_1 \rangle + \langle f_2, f_1 \rangle + \lambda_2 \lambda_1. \end{cases} \quad (11)$$

These equations are linear in  $w_2, f_2$ , with the same differential operator as for the first equations (10). The nonlinearity is accounted by the items  $w_1, f_1$  appearing in the bracket operators and the latter will be known after the resolution of a boundary value problem based on Eq.(10). The generic form of the linear problems at order  $K$  ( $K \geq 2$ ) is:

$$\begin{cases} D\Delta^2 w_K - [w_0, f_K] - [w_K, f_0] = \lambda_K p + g_K^{nl} \\ \frac{1}{Eh}\Delta^2 f_K + [w_0, w_K] = h_K^{nl} \\ 0 = \langle w_K, w_1 \rangle + \langle f_K, f_1 \rangle + \lambda_K \lambda_1, \end{cases} \quad (12)$$

where  $g_K^{nl} = \sum_{R=1}^{K-1} [w_R, f_{K-R}]$ ,  $h_K^{nl} = -(\sum_{R=1}^{K-1} [w_R, w_{K-R}])/2$ . Note that the

problems (11),(12), and the definitions of the right-hand-sides  $g_K^{nl}$  and  $h_K^{nl}$  follow from the well known Leibniz rule defining the high order derivatives of a product. This formula is written in terms of coefficients of power series:

$$(fg)_K = \sum_{R=0}^K f_R g_{K-R}. \quad (13)$$

This rule is not limited to products of real numbers, it holds also for scalar products of two vectors, for products of matrices, ..., and here for the bracket operator (2).

Because of linearity, the solution of (10) is in the form  $w_1(x, y) = \lambda_1 \hat{w}(x, y)$ ,  $f_1(x, y) = \lambda_1 \hat{f}(x, y)$ , where  $\hat{w}(x, y), \hat{f}(x, y)$  solve the following system:

$$\begin{cases} D\Delta^2 \hat{w} - [w_0, \hat{f}] - [\hat{w}, f_0] = p \\ \frac{1}{Eh} \Delta^2 \hat{f} + [w_0, \hat{w}] = 0 \end{cases} \quad (14)$$

The resolution of boundary value problems based on (14) will be discussed in Section 2.2 by the technique of Taylor series. The third equation in (10) yields the load parameter at order one:

$$\lambda_1^2 = \frac{1}{\langle \hat{w}, \hat{w} \rangle + \langle \hat{f}, \hat{f} \rangle + 1} \quad (15)$$

Eq.(15) has two solutions because one can move in two directions along the branch of solutions. In the first ANM-step, the user has to define the orientation. In the next ones, the orientation is chosen with respect to the tangent

direction at the end of the previous step, see [31].

For the generic case at order  $K$ ,  $K \geq 2$ , (Eq. (12)), there are three right hand sides,  $\lambda_K p(x, y)$  that is similar to the order one, and two new functions  $g_K^{nl}(x, y)$  and  $h_K^{nl}(x, y)$  that depend only on the unknowns at previous orders (orders  $\leq K - 1$ ): so the power series can be computed recurrently. Hence the solution at order  $K$  can be split in two parts:

$$\begin{cases} w_K = \lambda_K \hat{w} + w_K^{nl} \\ f_K = \lambda_K \hat{f} + f_K^{nl}, \end{cases} \quad (16)$$

where  $(\hat{w}, \hat{f})$  has been defined at the first order and  $(w_K^{nl}, f_K^{nl})$  is the solution of

$$\begin{cases} D\Delta^2 w_K^{nl} - [w_0, f_K^{nl}] - [w_K^{nl}, f_0] = g_K^{nl} \\ \frac{1}{Eh} \Delta^2 f_K^{nl} + [w_0, w_K^{nl}] = h_K^{nl}. \end{cases} \quad (17)$$

Thus, one has defined a family of linear PDEs (14)(17) that can be solved recurrently. To complete the boundary value problems, one generally needs to include the in-plane displacement at order  $K$ . First, the Taylor expansion of the constitutive law (6) provides a sequence of linearized equations:

$$\{\epsilon(\mathbf{u})\}_K + \frac{1}{2} \sum_{R=0}^K [A(\mathbf{g}_R)] \{g\}_{K-R} = [M] \{D^2 f\}_K \quad (18)$$

where  $\mathbf{g} = \nabla w$ . Solving the latter equation (18) will provide  $\mathbf{u}_K$ , the in-plane displacement at order  $K$ .

## 2.2. Taylor series with respect to space variables (TMM)

Next the linear equations (14) and (17) with variable coefficients are solved by Taylor meshless method (TMM). Within TMM, the boundary value problems are treated in two steps: first one computes the general solutions of the PDEs by the technique of Taylor series, which leads to a rather small number of shape functions, second the boundary and interface conditions are discretized by one of the techniques discussed in [49][56][50]. In this part, one begins with the solving procedure by Taylor series that is presented in the case of a system in the form:

$$\begin{cases} D\Delta^2 w - [w_0, f] - [w, f_0] = g \\ \frac{1}{Eh}\Delta^2 f + [w_0, w] = h, \end{cases} \quad (19)$$

which corresponds to (14) or (17). The functions  $w_0(x, y)$ ,  $f_0(x, y)$ ,  $g(x, y)$  and  $h(x, y)$  in (19) are given in the form of Taylor series. In each subdomain, the two unknowns  $w(x, y)$  and  $f(x, y)$  are approximated by Taylor series truncated at degree  $N$ :

$$\begin{Bmatrix} w(x, y) \\ f(x, y) \end{Bmatrix} = \sum_{m=0}^N \sum_{n=0}^{N-m} (x - x_0)^m (y - y_0)^n \begin{Bmatrix} w_{m,n} \\ f_{m,n} \end{Bmatrix} \quad (20)$$

Note that (20) is a discretization of the unknown fields  $w(x, y)$  and  $f(x, y)$ , the discrete variables being the  $(N + 1)(N + 2)$  Taylor coefficients  $w_{m,n}$  and  $f_{m,n}$ . Next one seeks approximated solutions of the equations (19) in the



sense of Taylor series by setting to zero the power series of the residual:

$$\begin{cases} D(\Delta^2 w)_{m,n} - [w_0, f]_{m,n} - [w, f_0]_{m,n} = g_{m,n} \\ \frac{1}{Eh}(\Delta^2 f)_{m,n} + [w_0, w]_{m,n} = h_{m,n} \end{cases} \quad (21)$$

for integers  $m$  and  $n$  such that  $0 \leq m + n \leq N - 4$ . So the PDEs (19) lead to the algebraic equations (21) satisfied by the Taylor coefficients  $w_{m,n}$  and  $f_{m,n}$ . It is the latter algebraic equations that are to be solved in order to reduce the number of discrete unknowns  $w_{m,n}$  and  $f_{m,n}$ .

The key points of the present procedure are to establish these discrete relations (21) and to solve them for reducing the number of unknowns. In order to establish these discrete equations, one relies on obvious properties of derivatives on one hand, and, on the other hand, on the 2D Leibniz formula that is given by:

$$(fg)_{m,n} = \sum_{m_1=0}^m \sum_{n_1=0}^n f_{m_1,n_1} g_{m-m_1,n-n_1} \quad (22)$$

First let us detail the computation of the Taylor coefficients of the bilaplacian

$$\begin{aligned} (\Delta^2 w)_{m,n} &= (m+4)(m+3)(m+2)(m+1)w_{m+4,n} \\ &\quad + 2(m+2)(m+1)(n+2)(n+1)w_{m+2,n+2} \\ &\quad + (n+4)(n+3)(n+2)(n+1)w_{m,n+4} \end{aligned} \quad (23)$$

as well as the tensor of the second derivatives

$$\{D^2w\}_{m,n} = \begin{Bmatrix} \partial^2 w / \partial x^2 \\ \partial^2 w / \partial y^2 \\ \partial^2 w / \partial x \partial y \end{Bmatrix}_{m,n} = \begin{Bmatrix} (m+2)(m+1)w_{m+2,n} \\ (n+2)(n+1)w_{m,n+2} \\ (m+1)(n+1)w_{m+1,n+1} \end{Bmatrix}. \quad (24)$$

Next one has to calculate the terms like  $[f, w_0]_{m,n}$  in the equation (21). In this respect, one applies the 2D Leibniz formula (22) to the matricial equation (7), which gives:

$$[A, B]_{m,n} = \sum_{m_1=0}^m \sum_{n_1=0}^{m-m_1} {}^t \{D^2 A\}_{m_1, n_1} \begin{bmatrix} 0 & 1 & 0 \\ 1 & 0 & 0 \\ 0 & 0 & -2 \end{bmatrix} \{D^2 B\}_{m-m_1, n-n_1}. \quad (25)$$

By combining (24) and (25), one is able to compute all the Taylor coefficients  $[f_0, w]_{m,n}$ ,  $[w, f_0]_{m,n}$ ,  $[w_0, w]_{m,n}$ . They are written as functions of the derivatives of the two unknowns  $w$  and  $f$  such that the order of the first index is lower than or equal to  $m+2$  (as compared with the bilaplacian term whose largest degree is  $m+4$ ). Because the right hand sides  $g_{m,n}$  and  $h_{m,n}$  are also built from bracket nonlinearities, they can be computed in the same way.

The relations (21) can be considered as recurrence formulas and they permit to build easily the family of polynomials that are solutions of the FvK equations within the approximation by Taylor series. Let us re-write

these equations as:

$$\begin{cases} \alpha Dw_{m+4,n} = -\beta Dw_{m+2,n+2} - \gamma Dw_{m,n+4} + [w_0, f]_{m,n} + [w, f_0]_{m,n} + g_{m,n} \\ \frac{\alpha}{Eh} f_{m+4,n} = -\frac{\beta}{Eh} f_{m+2,n+2} - \frac{\gamma}{Eh} f_{m,n+4} - [w_0, w]_{m,n} + h_{m,n}. \end{cases} \quad (26)$$

where  $\alpha = (m+4)(m+3)(m+2)(m+1)$ ,  $\beta = 2(m+2)(m+1)(n+2)(n+1)$ ,  $\gamma = (n+4)(n+3)(n+2)(n+1)$ . The latter relations define an affine subspace of polynomials that are easily computed because the right hand sides of (26) correspond to a first index lower or equal to  $m+2$ , while this index is equal to  $m+4$  in the left hand side. To generate this subspace of polynomials, let us assume that the following coefficients  $\{w_{0,n}, f_{0,n}, w_{1,n}, f_{1,n}, w_{2,n}, f_{2,n}, w_{3,n}, f_{3,n}\}$  are given. Clearly, all the other coefficients  $\{w_{m,n}, f_{m,n}\}$  for  $m \geq 4$  will be easily deduced from the recurrence formula (26):  $\{w_{4,n}, f_{4,n}\}$  from (26) for  $m = 0$ ,  $\{w_{5,n}, f_{5,n}\}$  from (26) for  $m = 1$ , etc. Let us introduce a vector  $\mathbf{c}$ :

$$\{c_1, c_2, c_3, c_4, c_5, \dots, c_{8N-4}\} = \{w_{0,0}, f_{0,0}, w_{1,0}, f_{1,0}, w_{0,1}, \dots\} \quad (27)$$

by collecting all the pairs  $\{w_{m,n}, f_{m,n}\}$  for  $0 \leq m \leq 3, m+n \leq N$ . To get a particular solution, one chooses  $\mathbf{c} = \mathbf{0}$  and one applies the recurrence formula (26): so one builds a pair of polynomials  $(\check{P}^w(x, y), \check{P}^f(x, y))$  that solves the FvK equations in the sense of Taylor series. To get the first solution of the homogeneous equations, let us choose  $g_{m,n} = 0, f_{m,n} = 0, c_1 = 1, c_k = 0$  for  $k \neq 1$ : then the application of the recurrence (26) yields a first pair of

polynomials  $(N_1^w(x, y), N_1^f(x, y))$ . A second pair of polynomial solution is obtained by choosing  $g_{m,n} = 0, f_{m,n} = 0, c_2 = 1, c_k = 0$  for  $k \neq 2$  and so on. Finally, all these applications of the recurrence formula permit to obtain all the polynomial solutions of the linearized FvK system (19):

$$w(x, y) = \check{P}^w(x, y) + \mathbf{c} \cdot \mathbf{N}^w(x, y) \quad (28)$$

$$f(x, y) = \check{P}^f(x, y) + \mathbf{c} \cdot \mathbf{N}^f(x, y). \quad (29)$$

As to the discretized in-plane displacement  $\mathbf{u}$ , it follows from the formula (18) whose discretization by power series in  $(x, y)$  leads to:

$$\left\{ \begin{array}{c} (m+1)u_{m+1,n}^K \\ (n+1)v_{m,n+1}^K \\ (m+1)v_{m+1,n}^K + (n+1)u_{m,n+1}^K \end{array} \right\} + \frac{1}{2} \sum_{R=0}^K \sum_{m_1=0}^m \sum_{n_1=0}^n [A(\mathbf{g}_{m_1,n_1}^R)] \{g_{m-m_1,n-n_1}^{K-R}\} = [M] \{D^2 f\}_{m,n}^K \quad (30)$$

If the main unknowns  $w, f$  and therefore  $\mathbf{g} = \nabla w$  are given in terms of Taylor series, the latter formula (30) provides the strain  $\epsilon$  and thus permits to build the Taylor coefficients of the in-plane displacement  $(u_{m,n}^K, v_{m,n}^K)$ , except the three first ones  $u_{0,0}^K, v_{0,0}^K$  and  $u_{0,1}^K = -v_{1,0}^K$ , which corresponds to a rigid body motion: these three quantities have to be added to the unknown vector  $\mathbf{c}$  in (27). Note that, with three equations for two unknowns  $u(x, y)$  and  $v(x, y)$ ,

the system (30) seems overdetermined, but the corresponding compatibility condition is the second FvK equation (1) that was previously solved.

### 2.3. Boundary and interface conditions

The method of Taylor series has permitted to solve the Föppl-Von Karman equations and such an approximated solution (28)(29) is valid in the whole domain or, at least, in a part of this domain. So, it remains to apply the boundary conditions and the transmission condition in cases where several Taylor series are needed. In this respect, several procedures are available, the earliest one being the hybrid-Trefftz method [40][42]. Various meshless methods have been proposed within TMM [48][49]. In this respect, we shall use a least-square collocation method that associates efficiency, robustness and simplicity as compared with alternative approaches [50] and it works well, even for problems requiring many subdomains [56][54].

For simplicity, the least-square boundary collocation method is described in the case of a simply supported square plate submitted to a uniaxial compressive stress  $\lambda$  as in Figure 1. The FvK model is coupled with the following boundary conditions:

$$\begin{aligned} x = \pm \frac{a}{2} : \quad w &= 0, & \frac{\partial^2 w}{\partial x^2} &= 0, & \frac{\partial^2 f}{\partial y^2} &= -\lambda h, & \frac{\partial^2 f}{\partial x \partial y} &= 0 \\ y = \pm \frac{a}{2} : \quad w &= 0, & \frac{\partial^2 w}{\partial y^2} &= 0, & \frac{\partial^2 f}{\partial x^2} &= 0, & \frac{\partial^2 f}{\partial x \partial y} &= 0. \end{aligned} \quad (31)$$

Note that the boundary conditions for the stress function  $f$  represent an

applied membrane stress around the domain. The same boundary conditions are valid at each order  $K$  of the ANM-expansion with  $[w(x, y), f(x, y), \lambda]$  replaced by  $[w_K(x, y), f_K(x, y), \lambda_K]$ . In section 3.1, this FvK boundary value problem will be discretized with a single domain, i.e. by a single Taylor series in the whole domain.

In order to satisfy the boundary conditions within the meaning of least-square collocation approach, one introduces a family of  $M$  collocation points  $(x_\alpha, y_\alpha)$  on the boundary (see figure 1), by distinguishing the sets of points  $\mathcal{I}_x$  and  $\mathcal{I}_y$  lying on the sides  $x = \pm \frac{a}{2}$  and  $y = \pm \frac{a}{2}$ . Next, one minimizes the following function (let us recall that the vector  $\mathbf{c}$  contains the free parameters generating the general solution of the PDEs, cf (28)(29):

$$J_{BC}(\mathbf{c}) = \sum_{\alpha \in \mathcal{I}_x} \left[ w^2 + \left( \frac{\partial^2 w}{\partial x^2} \right)^2 + \left( \frac{\partial^2 f}{\partial y^2} + \lambda_K h \right)^2 + \left( \frac{\partial^2 f}{\partial x \partial y} \right)^2 \right] (x_\alpha, y_\alpha) + \sum_{\beta \in \mathcal{I}_y} \left[ w^2 + \left( \frac{\partial^2 w}{\partial y^2} \right)^2 + \left( \frac{\partial^2 f}{\partial x^2} \right)^2 + \left( \frac{\partial^2 f}{\partial x \partial y} \right)^2 \right] (x_\beta, y_\beta) \quad (32)$$

Applications of this procedure to other boundary conditions are straightforward and have been detailed in the literature [56] [53]. For instance, with a clamped plate, one has to replace the second term in each bracket by the square of the normal derivative of the deflection  $w$ . One can also add weighting parameters in this function  $J_{BC}(\mathbf{c})$  to limit the ill-conditioning of the final problem. This minimization problem (32) leads to a linear system with a symmetric positive definite matrix. Note that this least-square collocation

method is used because the pure collocation method does not work [48]. Previous works [56] [50] have established that it converges and it is very robust if the number of collocation points is sufficiently large, the choice  $M \simeq 2N$  being quite secure.

The transmission conditions along interfaces between subdomains are written according to the same principle, some collocation points  $(x_\gamma, y_\gamma)$  being chosen along these interfaces. From a physical point of view, these transmission conditions concern the continuity of the displacement, of the rotation  $\frac{\partial w}{\partial \nu}$  and various components of the stress and moment tensors [62], but in the case of an isotropic homogeneous material as here, the transmission conditions are the continuity conditions of the main unknowns  $w$  and  $f$ , as well as of their first, second and third normal derivatives. The function to be minimized includes a part for the boundary conditions and a part for the transmission conditions, i.e.  $J(\mathbf{c}) = J_{BC}(\mathbf{c}) + J_{TR}(\mathbf{c})$ , where the transmission part can be written as:

$$\begin{aligned} J_{TR}(\mathbf{c}) = & \sum_{\gamma} \left\{ \llbracket w \rrbracket^2 + \llbracket \frac{\partial w}{\partial \nu} \rrbracket^2 + \llbracket \frac{\partial^2 w}{\partial \nu^2} \rrbracket^2 + \llbracket \frac{\partial^3 w}{\partial \nu^3} \rrbracket^2 \right\} (x_\gamma, y_\gamma) \\ & + \sum_{\gamma} \left\{ \llbracket f \rrbracket^2 + \llbracket \frac{\partial f}{\partial \nu} \rrbracket^2 + \llbracket \frac{\partial^2 f}{\partial \nu^2} \rrbracket^2 + \llbracket \frac{\partial^3 f}{\partial \nu^3} \rrbracket^2 \right\} (x_\gamma, y_\gamma). \end{aligned} \quad (33)$$

where the usual notation  $\llbracket . \rrbracket$  denotes a jump across the interface.

In this paper, we shall also study the boundary value problem in a square plate sketched in the figure 2, where, contrarily to the previous example, the in-plane displacement  $(u, v)$  is prescribed along the boundary (except  $u$

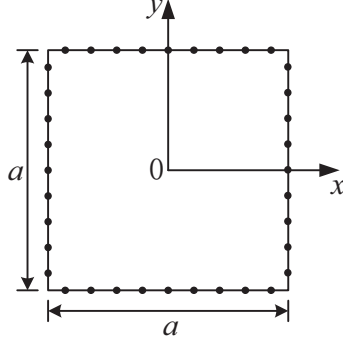


Figure 1: Simply supported square plate with boundary collocation points.

that is free along the horizontal lines). For this case of boundary conditions, the function (32) has to be modified to account for prescribed values of the in-plane displacement:

$$J_{BC}(\mathbf{c}) = \sum_{\alpha \in \mathcal{I}_x} \left[ (u \pm \lambda_K)^2 + v^2 + w^2 + \left( \frac{\partial^2 w}{\partial x^2} \right)^2 \right] (x_\alpha, y_\alpha) + \sum_{\beta \in \mathcal{I}_y} \left[ \sigma_{xy}^2 + v^2 + w^2 + \left( \frac{\partial^2 w}{\partial y^2} \right)^2 \right] (x_\beta, y_\beta) \quad (34)$$

A specific feature of Kirchhoff and FvK plate models is the corner condition that has to be prescribed, for instance in the case of a free boundary condition [63]. In the absence of concentrated force at the corner, the tangential bending moment  $m_{\nu\tau}$  must be continuous at the corner, what may be taken into account by adding a term  $K (\llbracket m_{\nu\tau} \rrbracket)^2$  to the function  $J_{BC}(\mathbf{c})$ ,  $K$  being a constant. This will be not necessary in the presented numerical tests, where only supported or clamped boundary conditions are considered.



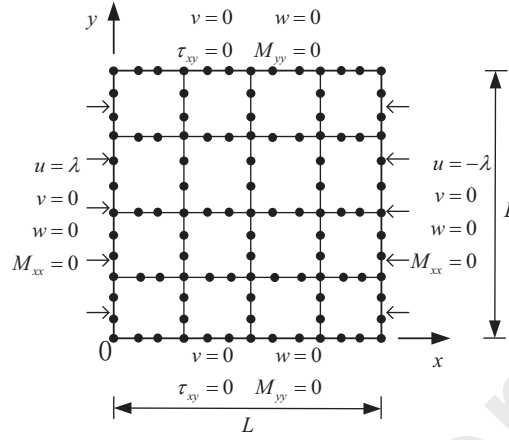


Figure 2: Boundary conditions for a square plate under uniaxial compression: simply supported and prescribed in-plane displacements. The plate is split in few large "elements". Collocation points are located on boundary and interfaces.

#### 2.4. ANM continuation and summary of the procedure

To solve a nonlinear boundary value problem depending on a parameter  $\lambda$ , a Taylor series expansion (ANM, formula (9)) with respect to a scalar parameter  $a$  has been applied in the section 2.1, which leads to a sequence of linearized partial differential systems (10)(12). Next, all these systems are solved by the Taylor meshless method (TMM): first, in each subdomain, the linearized PDEs are solved under the form of Taylor series with respect to the space variables  $(x, y)$ , which provides the unknown field by combining a particular solution and a number of shape functions, cf section 2.2; then, these Taylor series are assembled and boundary conditions are accounted for by using a least-square collocation technique, which solves the linearized systems (10)(12) and provides the double Taylor series (9)(20).

At this level, the solution path  $w(x, y, a)$ ,  $f(x, y, a)$ ,  $\lambda(a)$  is fully defined,

but not the range of validity  $a \in [0, a_{max}]$  of the Taylor series with respect to the path parameter. So, we have to define the range of validity of the series (9). In conformity with the basic ANM algorithm, one requires that the last term of the series is small with respect to the first one:

$$a_{\max} = \left\{ \delta \frac{\|\{f_1, w_1\}\|}{\|\{f_{N_a}, w_{N_a}\}\|} \right\}^{1/(N_a-1)} \quad (35)$$

In this way, the step length is defined a posteriori, i.e. from the computed Taylor series. Thus this leads to adaptive step lengths and this is very important when dealing with bifurcation problems. The radius of convergence is generally governed by the distance to the nearest bifurcation point [64]. That is why one observes an accumulation of small steps close to the bifurcation: hence, such an accumulation leads to a simple bifurcation criterion by sight, see for instance figure 4. Moreover, ANM permits to compute response curves with a very small perturbation force: one just has to choose a sufficiently small accuracy parameter  $\delta$ . Generally, this parameter  $\delta$  is the same for the whole calculation. A large value of  $\delta$  gives larger steps, but with a risk of inaccuracy, while a small  $\delta$  permits a more secure path following. So the choice of the parameter  $\delta$  is a key issue in the management of the calculation.

### 2.5. About the efficiency of the method

If the two computational techniques ANM and TMM were applied together only in the recent paper [57], much information about these two meth-

ods is available in the open literature, especially concerning ANM that was established 30 years ago and about which many papers were published. In practice, a sufficiently large order  $N_A \geq 10$  is generally chosen and, afterwards, the choice of this order is rather free, even if large orders  $N_A \geq 30, 40$  are recommended for large scale problems to optimize the computation time [35]. The key parameter is the number  $\delta$  that controls the step length, in particular when dealing with bifurcation problems, a small value of  $\delta$  avoiding unwanted branch switching.

There are much less papers about TMM, nevertheless its numerical efficiency has been assessed from a lot of numerical tests recently published in the literature. Many boundary value problems were considered, including linear problems (Laplace and Poisson equations, linear elasticity) [56][50] and nonlinear ones (nonlinear Poisson equations, hyperelastic bodies, Navier-Stokes equation) [53] [65] [54]. The main property of the TMM-discretization is the exponential convergence with the degree  $P$  up to large values  $P = 20$  or  $P = 30$ , as expected for Taylor series, but there is a limit beyond which the accuracy of the solver decreases. Such a behavior is due to the propagation of round-off errors and there is a connection with the ill-conditioning of the matrix, say a condition number larger than  $10^{20}$ , see [56] or [54] for more information. The same behavior was predicted by Schaback [66] in 1995 for the discretization by radial functions, in which case the numerical checking can be found in [55]. In other words, the number of shape functions in a subdomain (i.e. the degree  $P$ ) may be large, but not too large. In section 4,

a careful choice  $P = 8$  will be done to remain in the exponential convergence area and to avoid conditioning issues.

### 3. Numerical study of buckling problems

The numerical method of section 2 will be assessed by two examples concerning the buckling under uniaxial loading of a simply supported square plate whose side length is denoted by  $a$ . These two numerical tests are distinguished by the in-plane boundary conditions. We are interested in the convergence with respect to the degree ( $p$ -convergence) and to mesh refinement ( $h$ -convergence), as well as its ability to compute bifurcating curves with very small imperfections. Our numerical results will be compared with analytical and finite element results. The presented response curves will be expressed in terms of non-dimensional quantities  $\bar{w} = w/h$ ,  $\bar{\sigma} = \sigma a^2/Eh^2$  and  $\bar{p} = pa^4/Eh^4$ . Poisson's ratio is  $\nu = 0.3$ . The results will be presented in non-dimensional terms so that the chosen value of the Young modulus is ineffective.

#### 3.1. Buckling of a square plate under prescribed membrane forces

This boundary value problem has been presented in section 2.3. The boundary conditions (31) are expressed in terms of deflection  $w$  and stress function  $f$  and they correspond to prescribed in-plane stresses, the load parameter  $\lambda$  being the applied compressive stress in the x-direction. In this

case, we study the bifurcation load and the beginning of the post-bifurcation response up to  $\bar{w} \simeq 1$ . All the boundary conditions are accounted by least-square collocation with 240 collocation points. We use a single domain, which means a single Taylor series. The parameters of the algorithm are the ANM-degree  $K = 20$ , the spatial degree  $P = 20$ , which corresponds to 156 degrees of freedom, and the accuracy parameter  $\delta = 10^{-8}$  whose smallness is chosen to ensure the path-following for a quasi-perfect bifurcation. The results obtained by the presented method will be compared with finite element calculations done with the well-established code ANSYS. These two calculations need to input a small symmetry breaking. Within ANSYS, this is a small modal geometric imperfection measured by the initial displacement  $\bar{w}_{imp}$  called "scaling factor". Within the present method, a small transverse pressure  $\bar{p}$  will be introduced. The challenge is to perform a bifurcation analysis with a very small imperfection to get a response as close as possible to the perfect bifurcation.

The obtained bifurcation plots are presented in Figure 3 and Figure 4. Within ANSYS, we use a scaling factor of  $10^{-4}$  and  $10^{-6}$  and, within the present method, a dimensionless transversal pressure  $\bar{p} = 10^{-6}$ . ANSYS was not able to compute the bifurcating curve with a smaller imperfection, even if we suspect that some experts in non-linear calculation should be able to do such a calculation with a commercial package. Clearly, the new technique permitted us to compute the bifurcation plot with a very small imperfection simply by choosing a sufficiently large ANM degree and a sufficiently small

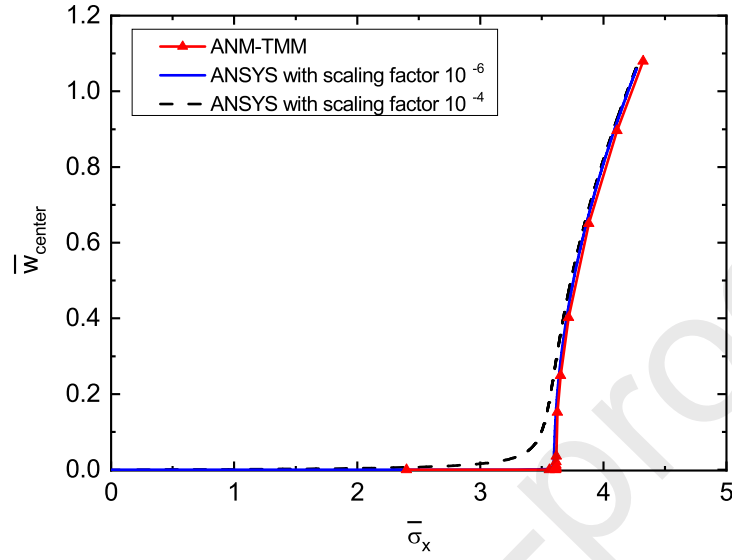


Figure 3: Buckling of a square plate under a prescribed uniaxial compressive force. Effect of small perturbations. The ANM-TMM algorithm is compared with a commercial finite element code. On the ANM-TMM curve, each point corresponds to one ANM step.

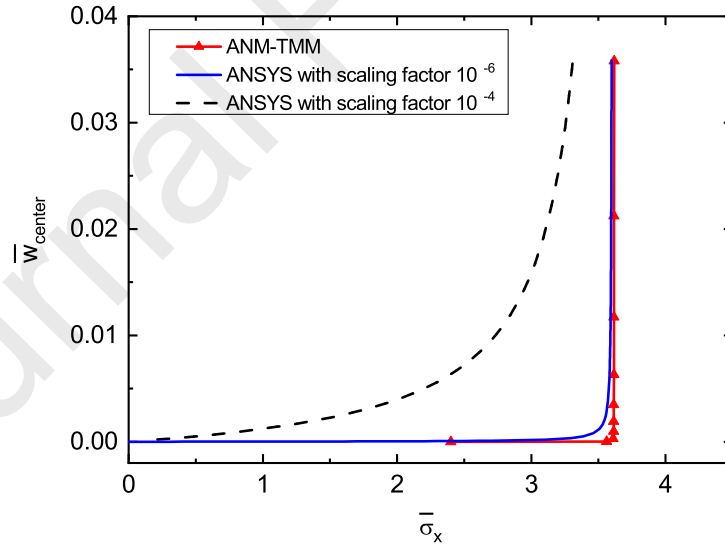


Figure 4: A zoom of Figure 3. One sees that the ANM-TMM method permits to compute easily quasi-perfect bifurcations. On the ANM-TMM curve, each point corresponds to one ANM step: this illustrates the step length adaptivity, especially its shortening near the bifurcation point.

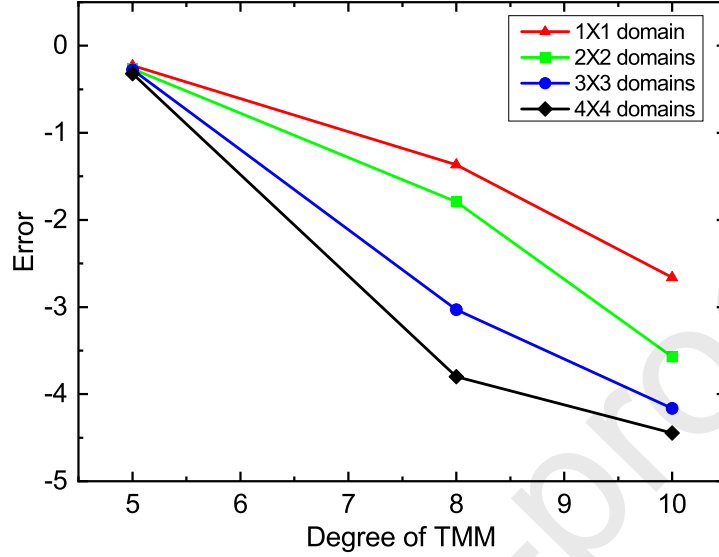


Figure 5: Buckling of a square plate under a prescribed uniaxial compressive force. The bifurcation stress is computed. One plots the decimal logarithm of the error versus degree ( $p$ -convergence) and number of subdomains ( $h$ -convergence).

accuracy parameter  $\delta$ .

Next, one discusses the convergence with the number of subdomains ( $h$ -convergence) and with the degree  $P$  of the polynomials ( $p$ -convergence). The interface and boundary conditions are accounted by the least-square collocation method in a similar way as in [56] and as described in section 2.3. One looks for the value of the bifurcation stress  $\bar{\sigma}_x$ . The analytic value  $\bar{\sigma}_x^{analytic}$  is 3.6152. One has applied TMM degrees  $P = 5, 8, 10$  and a number of subdomains varying from 1 to 16. The results are reported in Figure 5. Clearly, the method converges with the degree and/or with the number of subdomains, but very accurate results (i.e. error less than  $10^{-3}$ ) are obtained with 9 subdomains and  $P \geq 8$  or with 4 subdomains and  $P \geq 10$ .

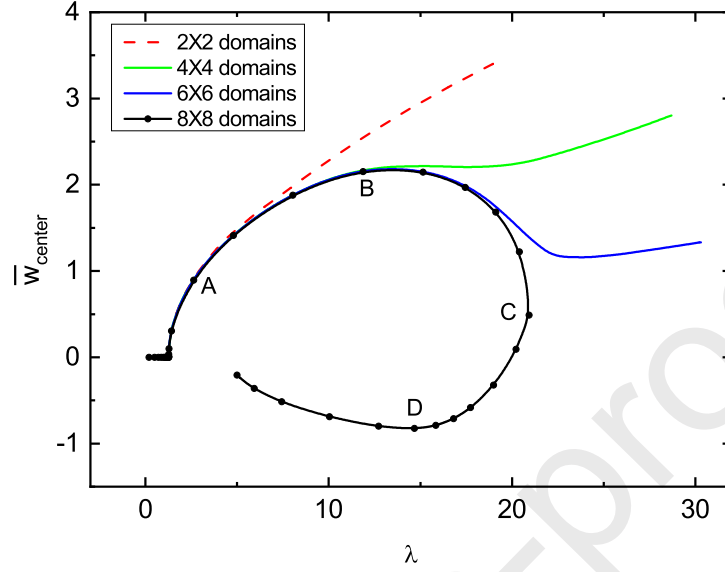


Figure 6: Compressed square plate, bifurcation plot, degree of TMM 8, order of ANM 10. Convergence with mesh refinement

### 3.2. Buckling of a square plate under prescribed in-plane displacements

One studies the second problem of a simply supported square plate described in section 2.3 and in figure 2. It differs from the previous case by the in-plane boundary conditions: normal displacements are prescribed,  $u = \lambda$  on the side  $x = -a/2$ ,  $u = -\lambda$  on the side  $x = a/2$  and  $v = 0$  on the sides  $y = \pm a/2$ . A tangential displacement  $v = 0$  is also prescribed on the vertical sides  $x = \pm a/2$ , the other boundary conditions being unchanged with respect to section 3.1. Contrarily to the previous example, large parts of the post-buckling range will be investigated, which will require a multi-domain discretization.

The parameters of the numerical procedure are chosen as follows. The symmetry breaking perturbation is represented by a very small transverse



uniform pressure  $\bar{p} = 10^{-6}$  and this requires a small value of the accuracy parameter  $\delta = 10^{-8}$  to ensure a path following able to capture the bifurcating curve. The order of the ANM-series is set to  $K = 10$  and the domain is split into  $N_e$  subdomains (that can be called "elements") with a Taylor series in each of them. The degree of the spatial approximation (TMM) will be generally chosen as  $P = 8$  or  $P = 10$ , which leads to  $N_e(8P - 4)$  degrees of freedom. The boundary conditions are accounted by least-square collocation with  $32P$  points in each "element", including the boundaries and the interfaces. The distribution of these points is shown in Figure 2.

To discuss the convergence of the method with the number of domains, several meshes  $2 \times 2$ ,  $4 \times 4$ ,  $6 \times 6$  and  $8 \times 8$  were used and the results are presented in figure 6. If the finest mesh  $8 \times 8$  is considered as a reference, the coarsest mesh is valid only just after the bifurcation ( $\bar{w} \leq 0.5$ ), the second one  $4 \times 4$  up to the point B and the third one  $6 \times 6$  a bit further. Four deformed shapes are presented in Figure 7. The bifurcation mode corresponds to a mode one (plot A of Figure 7) and the profile changes gradually towards a mode 3 (plot D of Figure 7), which requires a finer mesh.

Next, one keeps the finest mesh  $8 \times 8$  and Figure 8 compares the response curves obtained for the degrees 8 and 10 with the one computed by FEM. This FEM analysis is performed with the commercial software ANSYS using four-node element shell181. The plate is discretized with  $50 \times 50$  elements and LARGE DISPLACEMENT STATIC option is activated to perform a nonlinear analysis, which needs 15606 degrees of freedom. There are no

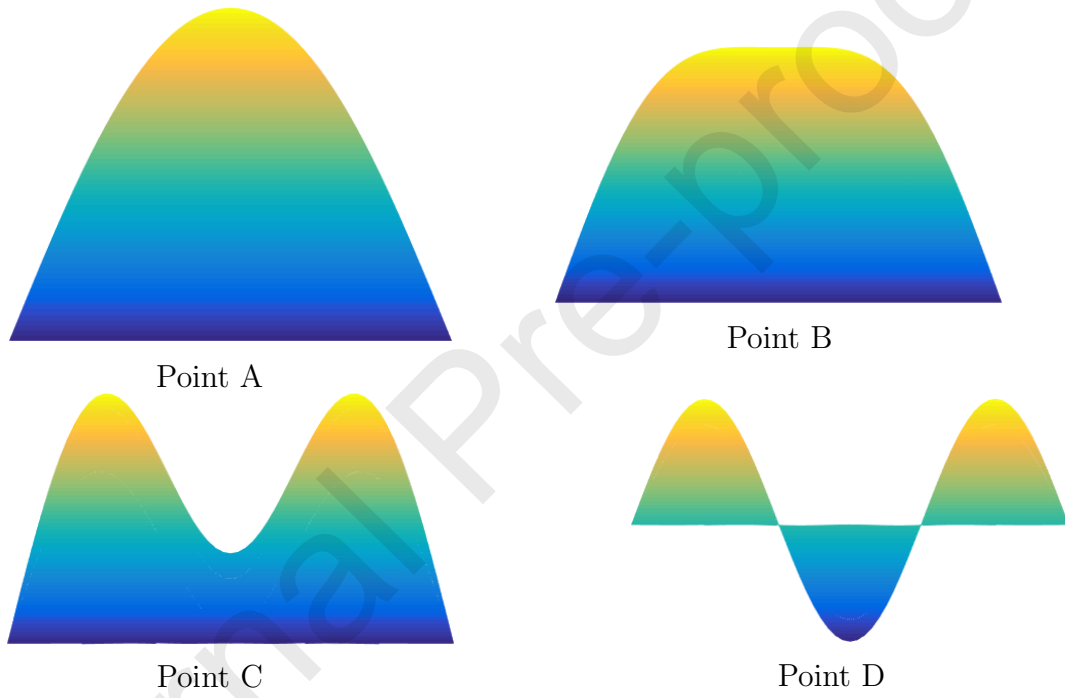


Figure 7: Deformed shapes along the x-axis of the plate at points A, B, C, D of Figure 6: one sees a transition from mode one to mode three. In this figure and in the following 3D plots, the colors represent the deflection  $w$ .

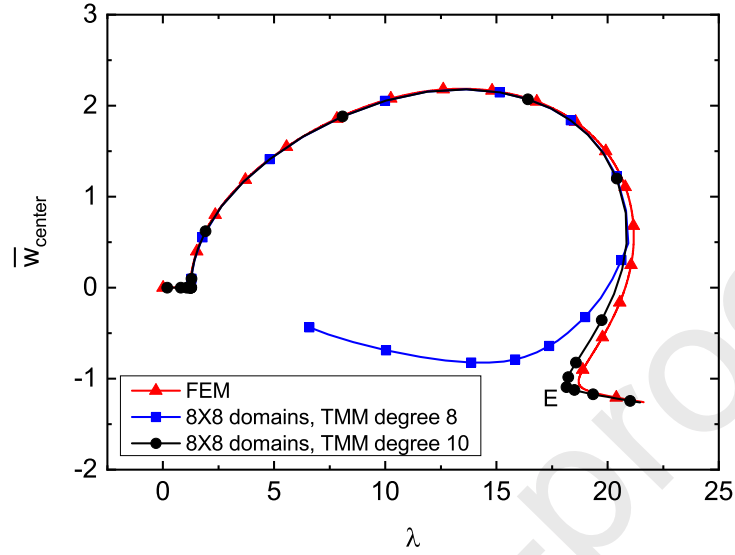


Figure 8: Compressed square plate, bifurcation plot, FEM versus TMM.

significant differences between the finite element results and those obtained with the degree  $P = 10$ , even after the secondary bifurcation near the point E. At this level, the plate has fully switched to mode 3, see figure 9.

Table 1 and Figure 10 present the applied displacement when the deflection of center point  $\bar{w}_{center} = 1$ . A degree  $P = 6$  is not sufficient to converge, even with  $8 \times 8$  domains. To improve the accuracy, one can increase either



Figure 9: Deformed shape at point E of Figure 8. The plate has switched to mode 3, as in the point D of Figure 7.

Table 1: Displacement load values when the displacement of center point is  $\bar{w} = 1$ . Convergence with mesh refinement and with the degree.

Number of subdomains	Degree of TMM					
	6	8	10	12	15	20
$2 \times 2$	3.14120	2.91440	3.00396	2.98004	2.98231	2.98268
$3 \times 3$	2.95625	2.98184	2.98279	2.98261	2.98263	2.98263
$4 \times 4$	2.96247	2.98271	2.98263	2.98262	2.98262	2.98262
$6 \times 6$	2.97156	2.98261	2.98262	2.98262	2.98262	2.98260
$8 \times 8$	3.00378	2.98261	2.98262	2.98262	2.98261	2.98260

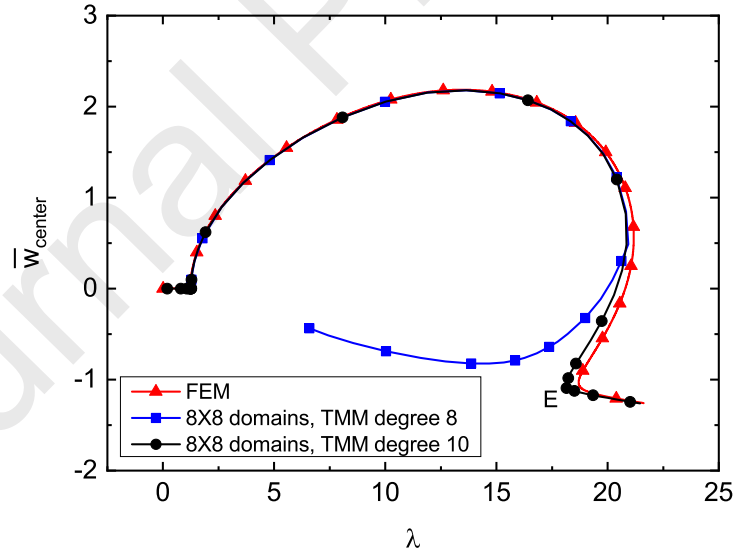


Figure 10: Applied shortening  $\lambda$  when the displacement of the center point  $\bar{w}$  is 1.

the degree of TMM or the number of domains. From the TMM results, the load to obtain  $\bar{w}_{center} = 1$  is  $\lambda = 2.98261 \pm 0.00002$ . From table 1, this optimal result can be reached with a degree  $P = 10$  and 16 "elements" or  $P = 12$  and only 9 "elements". The discrepancy between FEM and TMM is about  $3 \times 10^{-5}$ .

#### 4. Wrinkling of a rectangular sheet under shear loading

##### 4.1. Setting the problem

The asymptotic numerical method is a path following technique that proved to be a very robust continuation method. Thus, it seems natural to assess its behavior in the case of nearly slack membranes. In this respect, the very thin plate under shear loading studied by Wong and Pellegrino [23] is a representative example of nearly slack membrane. Numerical studies of this problem based on plate bending models can be found in [23][7], the nonlinear solver being the dynamic relaxation, and in [24][25][26], the solver being the Newton-Raphson algorithm. In all these papers, the pure shear loading problem is modified, generally by the introduction of a prescribed transverse pretensioning displacement, this transverse displacement changing significantly the wrinkling problem. Indeed in the small strain range, an applied shear leads to a tensile stress  $\sigma_+$  and to a compressive stress  $-\sigma_-$  that are very close ( $\sigma_+ \simeq \sigma_-$ ), which generates a nearly slack state of the membrane, while a wrinkled state requires a much larger tensile stress ( $\sigma_- \ll \sigma_+$ ). This applied pretensioning displacement increases significantly

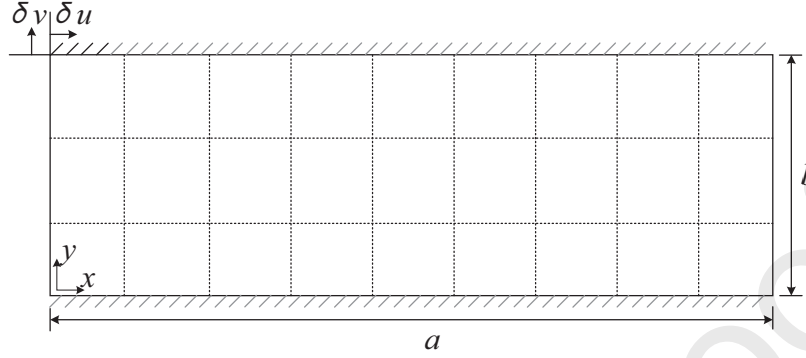


Figure 11: Rectangular membrane submitted to tension  $\delta v$  and shear load  $\delta u$ .

Table 2: Data, membrane under shear loading.

Width(mm)	$a$	380
Height(mm)	$b$	128
Thickness(mm)	$h$	0.025
Young's modulus(MPa)	$E$	3500
Poisson's ratio	$\nu$	0.3

the stiffness, which permits an easier start of the calculations. In this paper, the appearance of instability patterns will be simulated by the continuation method of Section 2, including for small shear strains and for very small prescribed pretensioning displacements.

The geometrical and material data are presented in figure 11 and table 2. They are exactly the same as in [23], with an aspect ratio  $a/b \simeq 3$  and a thickness ratio  $b/h = 5120$ . Similar data were used in other papers, but with a higher thickness ratio  $b/h = 8000$  in [25][26]. The membrane is simply supported along the short sides and clamped along the long sides. A vertical displacement  $\delta v$  is prescribed along the top side: this is the pretension load that was used to stabilize the membrane and to make easier the calculation.

The main loading is the shear that is applied via the prescribed horizontal displacement  $\delta u$ . These boundary conditions are summarized as:

$$\begin{aligned} w = 0 \quad \partial w / \partial y = 0 \quad u = 0 \quad v = 0 \quad (0 \leq x \leq a, y = 0) \\ w = 0 \quad \partial w / \partial y = 0 \quad u = \delta u \quad v = \delta v \quad (0 \leq x \leq a, y = b) \\ w = 0 \quad M_{xx} = 0 \quad \sigma_{xx} = 0 \quad \tau_{xy} = 0 \quad (x = 0, x = a, 0 \leq y \leq b) \end{aligned} \quad (36)$$

A small imperfection has to be added to detect bifurcation points and to follow bifurcating branches. We have seen in section 3 that this perturbation can be chosen very small when using the present numerical method. It is often defined as a geometrical imperfection in the procedures proposed by commercial codes. Here, for convenience, a small transversal pressure  $p(x, y)$  is introduced to create the wished initial loss of flatness, for instance in the wavy form in figure 12.

As in the previous studies about this shear problem, a multi-step strategy is necessary, as sketched in figure 13. The first step is the pretensioning of the membrane by applying the vertical displacement  $\delta v$ , which increases a little the very low initial stiffness. This step is followed by the application of the small transverse pressure  $p(x, y)$ . In this discussion, this imperfection will be represented by the deflection generated by this small pressure. The numerical process is closed by the main loading that is the shear generated by the horizontal displacement  $\delta u$ .

Contrarily to the previous authors, we investigate cases of nearly slack membranes, with a pretensioning load up to  $\delta v = 0.5\mu m$ , while the previous

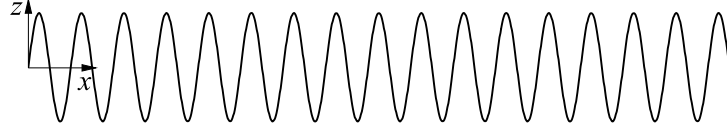


Figure 12: An example of pressure field  $p(x)$  to create an out-of-plane displacement.

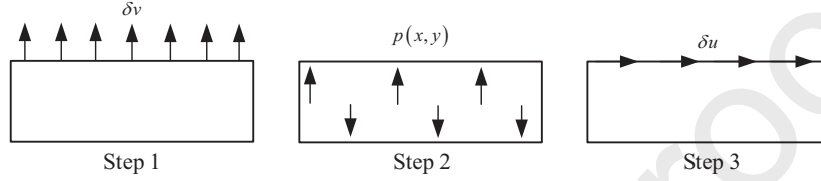


Figure 13: The three steps of the algorithm.

studies considered this pretensioning load in the range  $30\mu m - 100\mu m$ . In the same spirit, we focus on the initiation of the shear load in the range  $0 \leq \delta u \leq 0.15mm$ , while the other papers calculated directly the response to much larger loads.

#### 4.2. Adjusting the numerical model

Now we have to specify the parameters related to the numerical techniques. The asymptotic numerical method (ANM) needs two parameters: the degree of the Taylor series with respect to the load that is chosen as  $N_A = 10$  and the accuracy parameter  $\delta$  defined in (35) that is a crucial parameter to ensure the path-following in cases of sudden changes in the traveling direction. In the present case, a very small value is necessary and the same value  $\delta = 10^{-8}$  as in the buckling problems is chosen.

Next, the spatial discretization has to be defined. As in the p-version of the finite element method, this discretization involves a degree  $P$  and a



geometrical mesh. The degree  $P$  must be rather large to take advantage of the exponential convergence of Taylor series, but not too large because the matrix ill-conditioning leads to a loss of accuracy beyond some value of the degree: this behavior, known as "Schaback uncertainty principle", was discovered for radial basis functions [66][55] and established for discretization by Taylor series [56][54]. Thus, we limit ourselves to a spatial degree  $P = 8$ . The geometrical splitting conforms to almost the same rules as within finite element method, but with larger elements and a great freedom concerning their shapes. Simple splittings in rectangles as in figure 11 are used.

Various meshes have been tested in the case of a tension load  $\delta v = 0.02mm$ , of a shear load  $\delta u = 0.15mm$  and a small pressure able to generate a deflection of  $1\mu m$ :  $15 \times 5$ ,  $17 \times 6$ ,  $21 \times 7$ ,  $33 \times 11$ ,  $45 \times 15$  and  $63 \times 21$ . We were not able to get a consistent solution with the two coarsest meshes. With the mesh  $21 \times 7$ , the pattern of figure 14 is obtained where 8 wrinkles were observed. With the finer meshes  $33 \times 11$ ,  $45 \times 15$  and  $63 \times 21$ , the response of the membrane is stabilized at 11 wrinkles. Thus, we consider that the numerical process has converged and we shall use the mesh  $33 \times 11$  in the following calculations. This final pattern is plotted in figure 15. One remarks that the wrinkles are not uniformly distributed, their amplitude being larger near the edges. This amplifying effect of the boundary conditions has been observed in all the previous studies, except, of course, in the case of periodic boundary conditions [26].

Last, we have to fix the pressure  $p(x, y)$  to generate the initial imper-

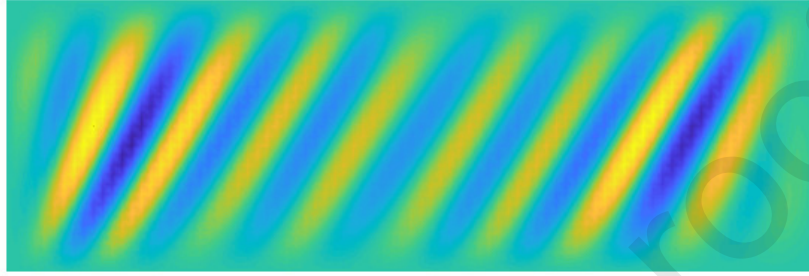


Figure 14: Test of the mesh  $21 \times 7$ . Tension load 0.02 mm, imperfection 0.001 mm, shear load 0.15 mm.

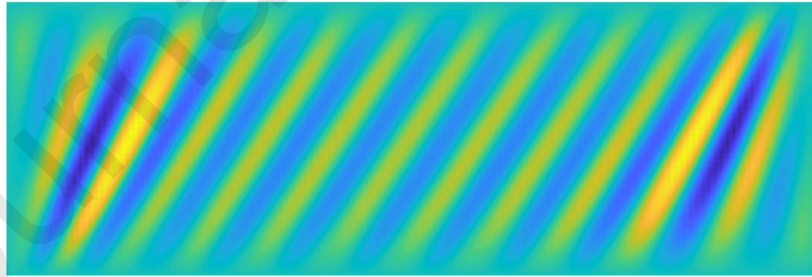


Figure 15: Wrinkled membrane with mesh  $33 \times 11$ , tension load 0.02 mm, imperfection 0.001 mm, shear load 0.15 mm.

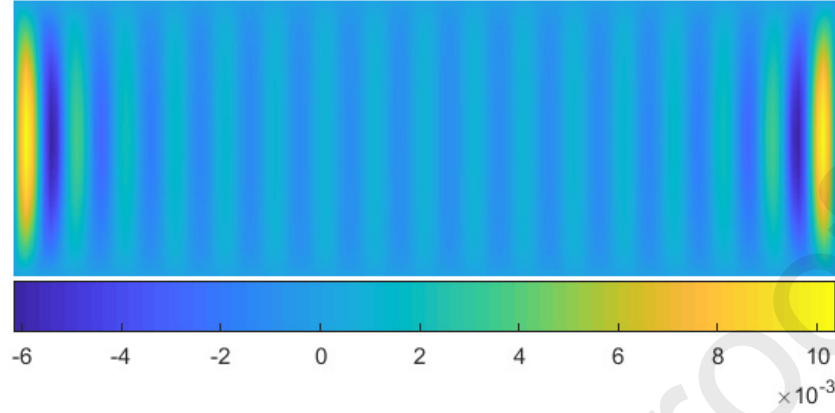


Figure 16: Geometric imperfection created by the pressure of figure 12.

fection permitting to follow the bifurcating branch. Periodic pressures as in figure 12 were applied with a pretension  $0.02mm$  and a mesh  $33 \times 11$ . A typical displacement after the second step is presented in figure 16. At this level, the deflection is small and one observes 16 vertical wrinkles, while the final shape in figure 15 involves 11 tilted wrinkles. This behavior is expected: the role of the imperfection is to trigger the bifurcation but the shape of the response is mainly governed by the instability mode and therefore it depends little on the imperfection. Several levels of imperfections were applied, from  $0.004h$  ( $0.1\mu m$ ) to  $0.32h$  ( $8\mu m$ ). With all these tests, 11 wrinkles were obtained, except with the largest imperfections  $0.2h$  (10 wrinkles) and  $0.32h$  (9 wrinkles). In what follows, an imperfection of  $1\mu m = 0.04h$  will be chosen.

#### 4.3. Effect of the prescribed transverse displacement

Response curves have been computed for a wide sample of prescribed transverse displacement  $\delta$ , from very small values  $\delta v = 0.5\mu m, 1\mu m$  up to

large values  $\delta v = 50\mu m, 80\mu m$ , the latter being in the range considered in the literature. Let us recall the main characteristics of our calculations: shear load  $\delta u \in [0, 150\mu m]$ , which is relatively small but covers a range ignored so far, imperfection  $1\mu m$ , degree of the spatial series  $P = 8$  and mesh  $33 \times 11$ .

Bifurcation plots are presented in figure 17 for six values of pretensioning load and the corresponding instability patterns in figure 18 for the maximal shear load  $\delta u = 150\mu m$ . Several rather surprising features have to be mentioned. If all the responses look like classical pitchfork bifurcation curves, the bifurcation load is very small for the lowest values of the pretension  $\delta v = 0.5\mu m, 1\mu m$ . The patterns associated with these small pretensions do not look like the one in figure 15 and those presented in the literature. There are only three and four wrinkles in the first cases  $\delta v = 0.5\mu m, 1\mu m$ , respectively, as compared with the 10 and 11 wrinkles occurring with the other values of the pretensioning, see figures 18c, 18d, 18e, 18f. So, the pretensioning load has a strong influence on the behavior of the membrane, at least for the smallest values of  $\delta v$ . For larger  $\delta v$ , the pattern seems stabilized and there are 11 wrinkles. Of course, a greater stiffness and therefore a smaller instability wavelength are found for larger values of the pretension, as expected. The existence of snap through is mentioned in the literature [23], which was associated with the appearance of new wrinkles [24], but we did not see such a phenomenon in the range of considered shear loads, the load-displacement relation being monotone after the bifurcation.

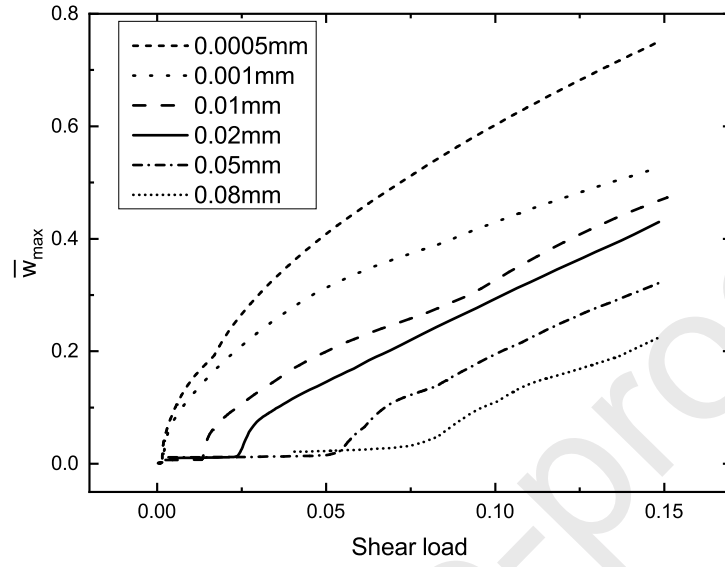


Figure 17: Bifurcation plots for various tension loads from 0.0005 mm to 0.08 mm. Shear load vs maximum displacement, imperfection 0.001 mm.

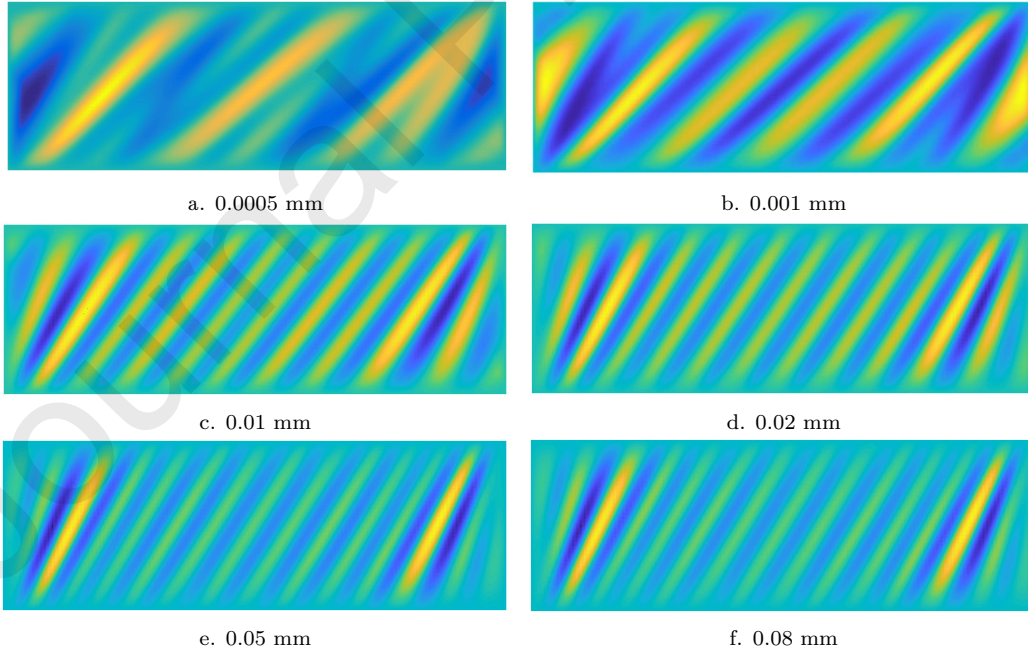


Figure 18: Wrinkle patterns with different tension loads.

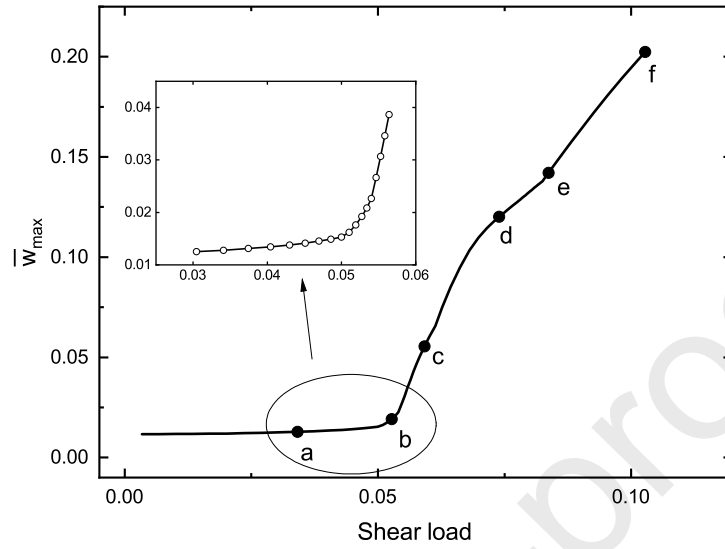


Figure 19: A zoom of the buckling curve, tension load 0.05 mm.

#### 4.4. Wrinkling initiation according to pretensioning load

Now we take a closer look near the bifurcation point to describe the generation of wrinkles. First, we begin by a case with a rather large tension of 0.05 mm. A zoom of the buckling curve with 0.05 mm tension load in figure 17 is shown in figure 19, the corresponding patterns being given in figure 20. For small shear load, the membrane remains flat, see points **a** and **b** and figures 20a and 20b. Next, the wrinkling patterns develop, first in a localized way, the membrane remaining quasi-flat in the center as in figures 20d and 20e. The appearance of wrinkles in the center begins in figure 20f and these central wrinkles develop and spread over the membrane up to a state as in figure 15.

This response of a membrane under large tension is now compared with two cases of nearly slack membranes, first with a membrane submitted to a

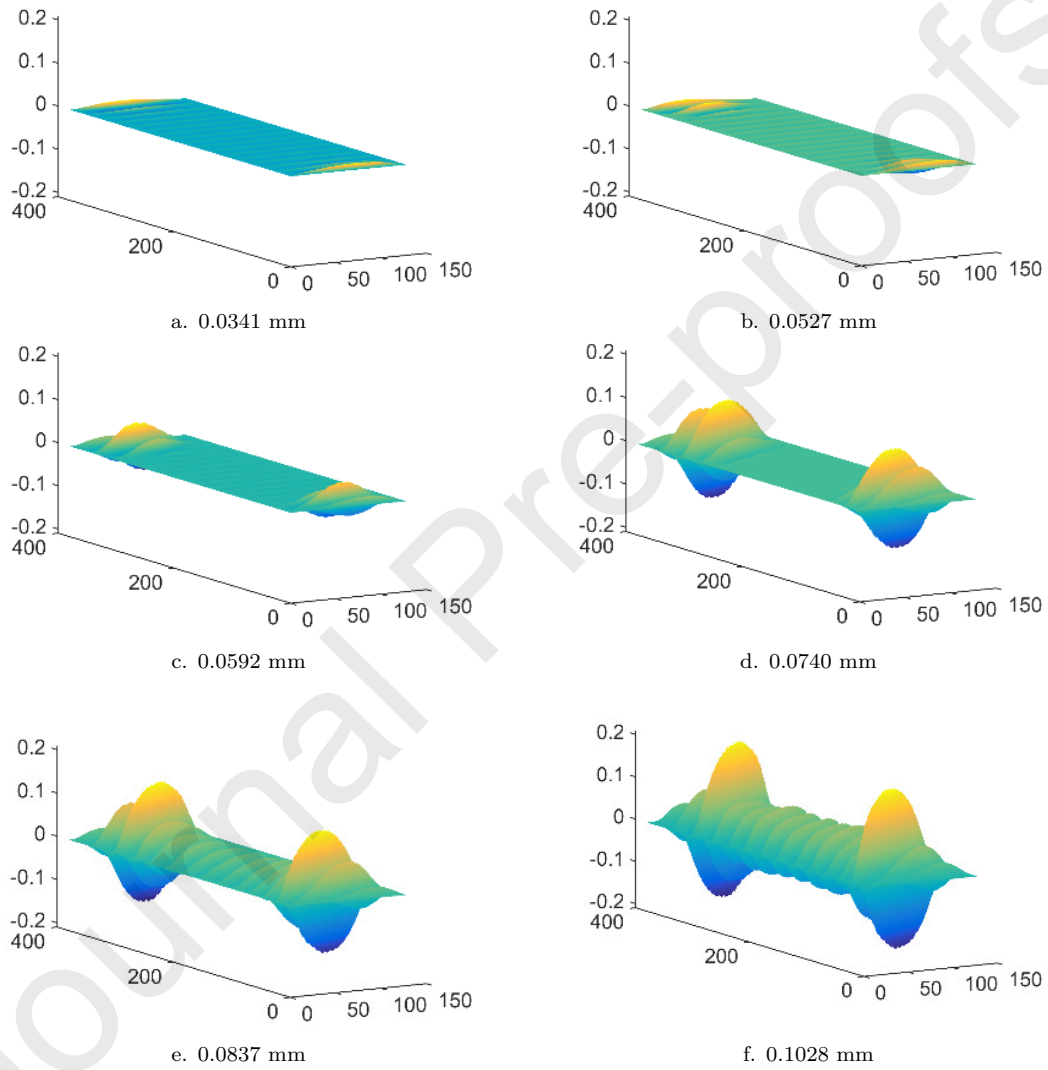


Figure 20: A large tension load 0.05 mm. Pattern evolution with increasing shear load.

very small tension  $\delta v = 1\mu m$ , i.e. 50 times smaller than for the previous case. The global response (cf figure 21) looks like a beautiful pitchfork bifurcation, even if the pre-bifurcation curve is less straight than in the large tension case. The bifurcation load  $\delta u = 0.0019mm$  is much smaller than for the large tension case  $\delta u \simeq 0.05mm$ . The wrinkling patterns are not localized near the edges as in the large tension case, but are more or less uniformly distributed in the membrane, from the bifurcation (figure 22b) up to fully developed wrinkles, see figures 22f and 18b.

Last, we have been able to compute the response curve for a very small tension  $\delta v = 0.5\mu m$ . We did not succeed for smaller values of the tension or without tension. Even in the present case  $\delta v = 0.5\mu m$ , we missed sometimes the bifurcation and several attempts were necessary to capture the bifurcating curve. The algorithm was tuned via the accuracy parameter  $\delta$  and the choice of the imperfection  $\bar{p}$ , the same adjustments (accuracy, imperfection) permitting also this control within classical incremental-iterative procedures. In the zoom of figure 23, there are several forward and backward motions before the main bifurcation (point **b**). The computation of this piece of curve required a lot of ANM steps, which confirms the difficulty of traveling through this region with very low tensile stress. The evolution of instability pattern is also erratic, even after the bifurcation at point **b**, with many shape changes. This shape seems finally stabilized with three wrinkles, for a shear displacement  $\delta u = 0.15mm$ , see figure 18a. This test illustrates the difficulty to follow the response curve when the membrane stress is very small. One



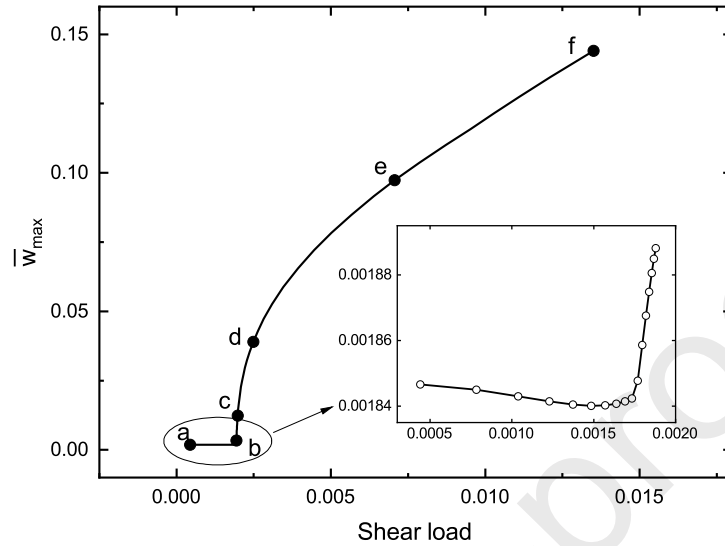


Figure 21: A zoom of the buckling curve, tension load 0.001 mm.

understands that an easier computational strategy would be to pass over this slack region and to go directly towards states where at least one principal stress is tensile and sufficiently large.

## 5. Conclusion

A new numerical procedure based on a technique of double Taylor series has been discussed in this paper: Taylor series with respect to a path parameter and Taylor series with respect to the space variables. The first Taylor series corresponds to the asymptotic numerical method (ANM) [30] and it transforms the nonlinear problem into a sequence of linearized equations satisfied by the Taylor coefficients. Next, these linear equations are solved in the form of a packet of spatial Taylor series, which corresponds to the Taylor meshless method (TMM) [54]. This procedure has been applied

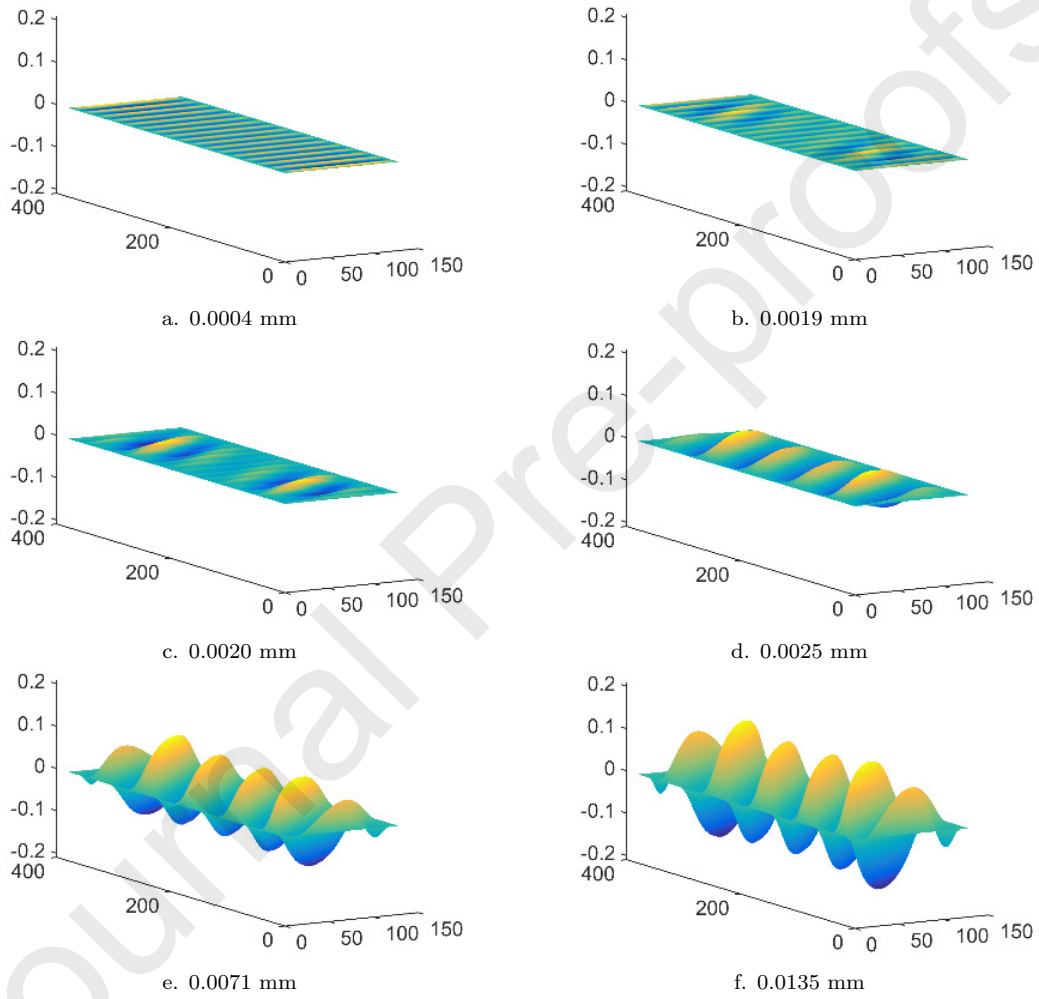


Figure 22: A very small tension load 0.001 mm. Pattern evolution with increasing shear load.

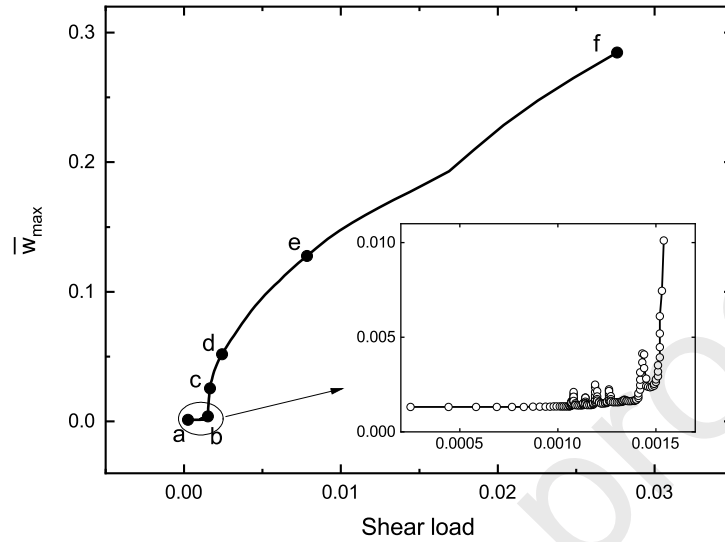
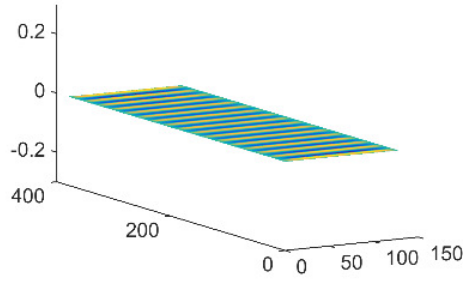


Figure 23: A zoom of the buckling curve, tension load 0.0005 mm.

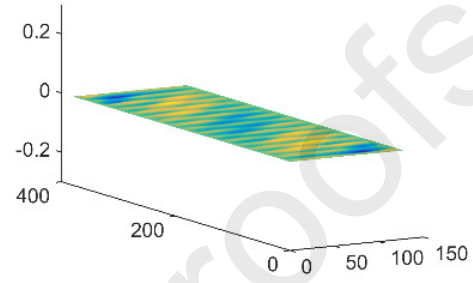
to the Föppl-von Karman plate equations.

The advantage of TMM is a strong reduction of the number of degrees of freedom, as compared with the finite element or finite difference method. The main numerical test was the wrinkling of a rectangular thin membrane submitted to shear loading [23]: it was solved with 363 "elements", i.e. 363 spatial Taylor series, which is much less than previous similar computations.

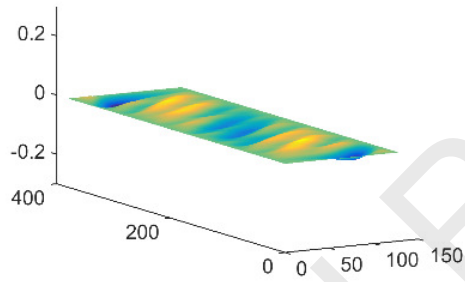
The advantage of ANM is to provide quite secure path-following procedures. That is why it has been assessed by numerical benchmarks known to be difficult to manage from this point of view: buckling problems with very small imperfections and the aforementioned wrinkling problem. In the literature, the latter problem is generally stabilized by a transverse pre-tensioning load and we have established that the tension modifies significantly the problem, the number of wrinkles decreasing strongly for a vanishing pre-



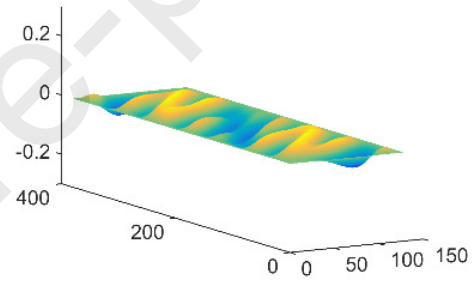
a. 0.0002 mm



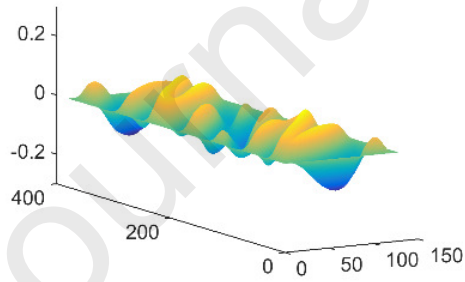
b. 0.0015 mm



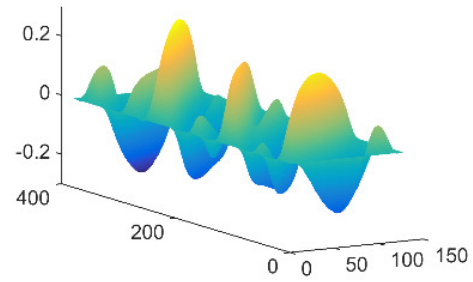
c. 0.0017 mm



d. 0.0024 mm



e. 0.0078 mm



f. 0.0276 mm

Figure 24: The smallest tension load 0.0005 mm. Pattern evolution with increasing shear load.

tension. These numerical tests prove that the response of difficult nonlinear problems can be computed by a path-following technique, in place of dynamic relaxation or in combination with it.

The proposed method is versatile and can be applied to a lot of nonlinear systems. For instance, there are applications to fluid mechanics of the asymptotic numerical method, e.g. [35] [16], and of the Taylor meshless method [65]. The automatic differentiation method [52] can be a help in case of more intricate equations, see for instance [53]. In this paper, we did not use the latter method, the Leibniz formula having permitted to compute all the power series we needed.

Consider, for example, hyperelastic models that have nowadays a lot of applications. A general procedure has yet to be established, but the basic rules are known. In this respect, the first idea is the quadratic recast [34][67], i.e. a transformation of the system of equations into a quadratic system, for instance  $y = x^3$  replaced by  $z = x^2$  and  $y = x \times z$ . Such a quadratic recast may be applied to any usual function, for instance  $y = e^x$  replaced by  $y' = y \times x'$ . A general account about this recast technique can be found in [68] and applications of ANM to hyperelastic problems are presented in [69][70][37] [38]. Once this transformation carried out, the recasted system can be solved by coupling ANM and TMM with the help of the Leibniz formula as in the present paper. The implementation can also be simplified by using an Automatic Differentiation toolbox, as done for ANM in [70] and for TMM in [53].

## Acknowledgments

Haitao Tian thanks the Chinese Science Council for his scholarship . The authors also acknowledge the support of the French government through the National Research Agency ANR (Labex DAMAS, Grant No.ANR-11-LABX-0008-01).

## References

- [1] E. Riks, An incremental approach to the solution of snapping and buckling problems, *International Journal of Solids and Structures* 15 (1979) 529–551.
- [2] H. B. Keller, *Lectures on Numerical Methods in Bifurcation Problems*, Springer-Verlag, Berlin, 1988.
- [3] A. Stanić, B. Brank, J. Korelc, On path-following methods for structural failure problems, *Computational Mechanics* 58 (2016) 281–306.
- [4] C. Y. Song, J. G. Teng, J. M. Rotter, Imperfection sensitivity of thin elastic cylindrical shells subject to partial axial compression, *International Journal of Solids and Structures* 41 (2004) 7155–7180.
- [5] N. Bowden, S. Brittain, A. G. Evans, J. W. Hutchinson, G. M. Whitesides, Spontaneous formation of ordered structures in thin films of metals supported on an elastomeric polymer, *Nature* 393 (1998) 146–149.

- [6] E. M. Haseganu, D. J. Steigmann, Analysis of partly wrinkled membranes by the method of dynamic relaxation, *Computational Mechanics* 14 (1994) 596–614.
- [7] M. Taylor, K. Bertoldi, D. J. Steigmann, Spatial resolution of wrinkle patterns in thin elastic sheets at finite strain, *Journal of the Mechanics and Physics of Solids* (2014) 163–180.
- [8] M. Taylor, B. Davidovitch, Z. Qiu, K. Bertoldi, A comparative analysis of numerical approaches to the mechanics of elastic sheets, *Journal of the Mechanics and Physics of Solids* 79 (2015) 92–107.
- [9] Z. Y. Huang, W. Hong, Z. Suo, Nonlinear analyses of wrinkles in a film bonded to a compliant substrate, *Journal of the Mechanics and Physics of Solids* 53 (2005) 2101–2118.
- [10] C. Fu, F. Xu, Y. Huo, Photo-controlled patterned wrinkling of liquid crystalline polymer films on compliant substrates, *International Journal of Solids and Structures* 132 (2018) 264–277.
- [11] N. Damil, M. Potier-Ferry, H. Hu, Membrane wrinkling revisited from a multi-scale point of view, *Advanced Modeling and Simulation in Engineering Sciences* 1 (2014) 6.
- [12] R. Seydel, Numerical computation of branch points in nonlinear equations, *Numerische Mathematik* 33 (1979) 339–352.

- [13] E. H. Boutyour, H. Zahrouni, M. Potier-Ferry, M. Boudi, Bifurcation points and bifurcated branches by an asymptotic numerical method and Padé approximants, *International Journal for Numerical Methods in Engineering* 60 (2004) 1987–2012.
- [14] Y. Guevel, H. Boutyour, J. M. Cadou, Automatic detection and branch switching methods for steady bifurcation in fluid mechanics, *Journal of Computational Physics* 230 (2011) 3614–3629.
- [15] B. Cochelin, M. Medale, Power series analysis as a major breakthrough to improve the efficiency of asymptotic numerical method in the vicinity of bifurcations, *Journal of Computational Physics* 236 (2013) 594–607.
- [16] Y. Guevel, T. Allain, G. Girault, J. M. Cadou, Numerical bifurcation analysis for 3-dimensional sudden expansion fluid dynamic problem, *International Journal for Numerical Methods in Fluids* 87 (2018) 1–26.
- [17] M. Taylor, M. Shirani, Y. Dabiri, J. M. Guccione, D. J. Steigmann, Finite elastic wrinkling deformations of incompressible fiber-reinforced plates, *International Journal of Engineering Science* 144 (2019) 103138.
- [18] R. Rossi, M. Lazzari, R. Vitaliani, E. Oñate, Simulation of light-weight membrane structures by wrinkling model, *International Journal for Numerical Methods in Engineering* 62 (2005) 2127–2153.
- [19] J. Rodriguez, G. Rio, J. M. Cadou, J. Troufflard, Numerical study of dynamic relaxation with kinetic damping applied to inflatable fabric



- structures with extensions for 3D solid element and non-linear behavior, *Thin-Walled Structures* 49 (2011) 1468–1474.
- [20] M. Lavrenčič, B. Brank, M. Brojan, Multiple wrinkling mode transitions in axially compressed cylindrical shell-substrate in dynamics, *Thin-Walled Structures* 150 (2020) 106700.
- [21] W. Wong, S. Pellegrino, Wrinkled membranes I: experiments, *Journal of Mechanics of Materials and Structures* 1 (2006) 3–25.
- [22] W. Wong, S. Pellegrino, Wrinkled membranes II: analytical models, *Journal of Mechanics of Materials and Structures* 1 (2006) 27–61.
- [23] W. Wong, S. Pellegrino, Wrinkled membranes III: numerical simulations, *Journal of Mechanics of Materials and Structures* 1 (2006) 63–95.
- [24] C. G. Wang, L. Lan, H. F. Tan, Secondary wrinkling analysis of rectangular membrane under shearing, *International Journal of Mechanical Sciences* 75 (2013) 299–304.
- [25] K. Senda, M. Petrovic, K. Nakanishi, Wrinkle generation without bifurcation in a shear-enforced rectangular membrane with free boundaries, *Journal of Spacecraft and Rockets* 52 (2015) 1057–1073.
- [26] K. Senda, M. Petrovic, K. Nakanishi, Localized wrinkle behavior near fixed boundaries in flat and cylindrical membranes, *Journal of Spacecraft and Rockets* 52 (2015) 1074–1090.

- [27] F. Xu, S. Zhao, C. Lu, M. Potier-Ferry, Pattern selection in core-shell spheres, *Journal of the Mechanics and Physics of Solids* 137 (2020) 103892.
- [28] T. Veldin, B. Brank, M. Brojan, Computational finite element model for surface wrinkling of shells on soft substrates, *Communications in Nonlinear Science and Numerical Simulation* 78 (2019) 104863.
- [29] T. Veldin, M. Lavrenčič, B. Brank, M. Brojan, A comparison of computational models for wrinkling of pressurized shell-core systems, *International Journal of Non-Linear Mechanics* 127 (2020) 103611.
- [30] B. Cochelin, N. Damil, M. Potier-Ferry, The asymptotic-numerical method: an efficient perturbation technique for nonlinear structural mechanics, *Revue Européenne des Éléments Finis* 3 (1994) 281–297.
- [31] B. Cochelin, A path-following technique via an asymptotic-numerical method, *Computers and Structures* 53 (1994) 1181–1192.
- [32] B. Cochelin, N. Damil, M. Potier-Ferry, Asymptotic-numerical methods and Padé approximants for non-linear elastic structures, *International journal for numerical methods in engineering* (1994) 1187–1213.
- [33] B. Cochelin, N. Damil, M. Potier-Ferry, *Méthode asymptotique numérique*, Hermes Lavoisier, Paris, 2007.
- [34] M. Potier-Ferry, N. Damil, B. Braikat, J. Descamps, J. M. Cadou, H. L. Cao, A. Elhage-Hussein, *Traitement des fortes non-linéarités par*

- la méthode asymptotique numérique, *Comptes Rendus de l'Académie des Sciences, Séries IIB* 324 (1997) 171–177.
- [35] M. Médale, B. Cochelin, A parallel computer implementation of the asymptotic numerical method to study thermal convection instabilities, *Journal of Computational Physics* 228 (2009) 8249–8262.
- [36] A. Timesli, B. Braikat, H. Lahmam, H. Zahrouni, A new algorithm based on moving least square method to simulate material mixing in friction stir welding, *Engineering Analysis with Boundary Elements* 50 (2015) 372–380.
- [37] O. Askour, A. Tri, B. Braikat, H. Zahrouni, M. Potier-Ferry, Method of Fundamental Solutions and high order algorithm to solve nonlinear elastic problems, *Engineering Analysis with Boundary Elements* 89 (2018) 25–35.
- [38] C. Fu, T. Wang, F. Xu, Y. Huo, M. Potier-Ferry, A modeling and resolution framework for wrinkling in hyperelastic sheets at finite membrane strain, *Journal of the Mechanics and Physics of Solids* 124 (2019) 446–470.
- [39] E. Trefftz, Ein Gegenstück zum Ritzschen Verfahren, in: *Proc. 2nd Int. Cong. Appl. Mech.*, Zurich, 1928, pp. 131–137.
- [40] E. Kita, N. Kamiya, Trefftz method: an overview, *Advances in Engineering Software* 24 (1995) 3–12.

- [41] J. Jirousek, N. Leon, A powerful finite element for plate bending, *Computer Methods in Applied Mechanics and Engineering* 12 (1977) 77–96.
- [42] J. Jirousek, A. P. Zieliński, Survey of Trefftz-type element formulations, *Computers and Structures* 63 (1997) 225–242.
- [43] H. Riou, P. Ladevèze, L. Kovalevsky, The Variational Theory of Complex Rays: An answer to the resolution of mid-frequency 3D engineering problem, *Journal of Sound and Vibration* 332 (2013) 1947–1960.
- [44] C. S. Chen, C. M. Fan, J. Monroe, The method of fundamental solutions for solving elliptic partial differential equations with variable coefficients, in: C. S. Chen, A. Karageorghis, Y. S. Smyrlis (Eds.), *The method of fundamental solutions-a meshless method*, Dynamic Publishers, Atlanta, 2008, pp. 75–105.
- [45] C. J. S. Alves, On the choice of source points in the method of fundamental solutions, *Engineering Analysis with Boundary Elements* 33 (2009) 1348–1361.
- [46] J. A. Kolodziej, A. P. Zieliński, *Boundary Collocation Techniques and their Application in Engineering*, WIT press, Southampton, 2009.
- [47] J. Jirousek, L. Guex, The hybrid-Trefftz finite element model and its application to plate bending, *International Journal for Numerical Methods in Engineering* 23 (1986) 651–693.

- [48] D. S. Zézé, M. Potier-Ferry, N. Damil, A boundary meshless method with shape functions computed from the PDE, *Engineering Analysis with Boundary Elements* 34 (2010) 747–754.
- [49] Y. Tampango, M. Potier-Ferry, Y. Koutsawa, S. Tiem, Coupling of polynomial approximations with application to a boundary meshless method, *International Journal for Numerical Methods in Engineering* 95 (2013) 1094–1112.
- [50] J. Yang, H. Hu, M. Potier-Ferry, Least-square collocation and Lagrange multipliers for Taylor meshless method, *Numerical Methods for Partial Differential Equations* 35 (2019) 84–113.
- [51] L. B. Rall, *Automatic differentiation-technique and applications*, Springer-Verlag, Berlin, 1981.
- [52] A. Griewank, A. Walther, *Evaluating derivatives: principles and techniques of algorithmic differentiation*, Society for Industrial and Applied Mathematics, Philadelphia, 2008.
- [53] J. Yang, H. Hu, Y. Koutsawa, M. Potier-Ferry, Taylor meshless method for solving non-linear partial differential equations, *Journal of Computational Physics* 348 (2017) 385–400.
- [54] J. Yang, M. Potier-Ferry, K. Akpama, H. Hu, Y. Koutsawa, H. Tian, D. S. Zézé, Trefftz methods and Taylor series, *Archives of Computational Methods in Engineering* 27 (2020) 673–690.

- [55] A. H. D. Cheng, M. A. Golberg, E. J. Kansa, G. Zang, Exponential convergence and Hc multiquadric collocation method for partial differential equations, *Numerical Methods for Partial Differential Equations* 19 (2003) 571–594.
- [56] J. Yang, H. Hu, M. Potier-Ferry, Solving large scale problems by Taylor Meshless Method, *International Journal for Numerical Methods in Engineering* 112 (2017) 103–124.
- [57] H. Tian, M. Potier-Ferry, F. Abed-Meraim, A numerical method based on Taylor series for bifurcation analyses within Föppl–von Karman plate theory, *Mechanics Research Communications* 93 (2018) 154–158.
- [58] A. Föppl, *Die wichtigsten Lehren der höheren Elastizitätstheorie*, Vol. 5, BG Teubner, Leipzig, 1907.
- [59] P. G. Ciarlet, A justification of the von Karman equations, *Archive for Rational Mechanics and Analysis* 73 (1980) 349–389.
- [60] T. J. Healey, Q. Li, R. B. Cheng, Wrinkling behavior of highly stretched rectangular elastic films via parametric global bifurcation, *Journal of Nonlinear Science* 23 (2013) 777–805.
- [61] H. Mottaqui, B. Braikat, N. Damil, Discussion about parameterization in the asymptotic numerical method: application to nonlinear elastic shells, *Computer Methods in Applied Mechanics and Engineering* 199 (2010) 1701–1709.

- [62] J. N. Reddy, Mechanics of laminated composite plates and shells: theory and analysis, CRC press, Boca Raton, 2003.
- [63] J. N. Reddy, Theory and analysis of elastic plates and shells, CRC press, Boca Raton, 2006.
- [64] S. Baguet, B. Cochelin, On the behaviour of the ANM continuation in the presence of bifurcations, International Journal for Numerical Methods in Biomedical Engineering 19 (2003) 459–471.
- [65] J. Yang, M. Potier-Ferry, H. Hu, Solving the stationary Navier–Stokes equations by using Taylor meshless method, Engineering Analysis with Boundary Elements 98 (2019) 8–16.
- [66] R. Schaback, Error estimates and condition numbers for radial basis function interpolation, Advances in Computational Mathematics 3 (1995) 251–264.
- [67] B. Cochelin, C. Vergez, A high order purely frequency-based harmonic balance formulation for continuation of periodic solutions, Journal of Sound and Vibration 324 (2009) 243–262.
- [68] L. Guillot, B. Cochelin, C. Vergez, A generic and efficient Taylor series based continuation method using a quadratic recast of smooth nonlinear systems, International Journal for Numerical Methods in Engineering 119 (2019) 261–280.

- [69] S. Nezamabadi, H. Zahrouni, J. Yvonnet, Solving hyperelastic material problems by asymptotic numerical method, *Computational mechanics* 47 (2011) 77–92.
- [70] F. Xu, Y. Koutsawa, M. Potier-Ferry, S. Belouettar, Instabilities in thin films on hyperelastic substrates by 3D finite elements, *International Journal of Solids and Structures* 69-70 (2015) 71–85.